REPORT DOCUMENTATION PAGE

Form Approved
OMB NO. 0704-0188

1. AGENCY USE ONLY *(Leave blank)*	2. REPORT DATE	3. REPORT TYPE AND DATES COVERED
	March 12, 1999	Final Report 1/3/95 - 30/11/98

4. TITLE AND SUBTITLE

Flamelet Surface Density and Burning Rate Integral in Premixed Combustion

5. FUNDING NUMBERS

DAAH04-95-1-0109

6. AUTHOR(S)

F. C. Gouldin

7. PERFORMING ORGANIZATION NAMES(S) AND ADDRESS(ES)

Cornell University
Ithaca, NY 14853-7501

8. PERFORMING ORGANIZATION REPORT NUMBER

9. SPONSORING / MONITORING AGENCY NAME(S) AND ADDRESS(ES)

U.S. Army Research Office
P.O. Box 12211
Research Triangle Park, NC 27709-2211

10. SPONSORING / MONITORING AGENCY REPORT NUMBER

ARO 33144.10-EG

11. SUPPLEMENTARY NOTES

The views, opinions and/or findings contained in this report are those of the author(s) and should not be construed as an official Department of the Army position, policy or decision, unless so designated by other documentation.

12a. DISTRIBUTION / AVAILABILITY STATEMENT

Approved for public release; distribution unlimited.

12 b. DISTRIBUTION CODE

13. ABSTRACT ***(Maximum 200 words)***

We have developed, tested and applied in V-flames and a spark ignition engine a new experimental method, crossed-plane laser imaging, for measuring flamelet surface normals in premixed turbulent flames. The method consists of taking simultaneous planar images in two orthogonal, laser illumination planes, and finding the flamelet normal at points along the line of intersection between the two planes where the flamelet crosses the line. In each image, the curve of intersection between the flamelet and the laser illumination plane is determined. Tangents to these curves are tangents to the flamelet surface, and where flamelet curves in the two illumination planes intersect, the normal is obtained from the cross product of the intersecting tangent lines. Flamelet data obtained with the method are used to determine probability density functions of normals, flamelet crossing densities, flamelet surface densities, and estimates of the burning rate integral.

In addition, two-component laser Doppler velocimetry has been combined with compensated fine-wire thermocouple thermometry to obtain mass flux data required for calculating the burning rate integral. Measurements have been made on several methane-air V-flames. The results demonstrate the utility of the method and the potential for turbulent burning velocity data to over estimate the acceleration of combustion by turbulence. Also, the performance of ionization probes in premixed turbulent flame studies was evaluated.

14. SUBJECT TERMS	15. NUMBER IF PAGES
	64
	16. PRICE CODE

17. SECURITY CLASSIFICATION OR REPORT	18. SECURITY CLASSIFICATION OF THIS PAGE	19. SECURITY CLASSIFICATION OF ABSTRACT	20. LIMITATION OF ABSTRACT
UNCLASSIFIED	UNCLASSIFIED	UNCLASSIFIED	UL

FLAMELET SURFACE DENSITY AND BURNING RATE INTEGRAL IN PREMIXED COMBUSTION

FINAL REPORT

F. C. Gouldin

12 March 1999

US Army Research Office

ARO Grant Number DAAH04-95-1-0109
1 March 1995 - 30 November 1998

Mechanical and Aerospace Engineering
Cornell University
Ithaca, NY 14853

Approved for Public Release
Distribution Unlimited

FLAMELET SURFACE DENSITY AND BURNING RATE INTEGRAL IN PREMIXED COMBUSTION

FINAL REPORT

F. C. Gouldin
Mechanical and Aerospace Engineering
Cornell University
Ithaca, NY 14853

ABSTRACT

We have developed, tested and applied in V-flames and a spark ignition engine a new experimental method, crossed-plane laser imaging, for measuring flamelet surface normals in premixed turbulent flames. The method consists of taking simultaneous planar images in two orthogonal, laser illumination planes, and finding the flamelet normal at points along the line of intersection between the two planes where the flamelet crosses the line. In each image, the curve of intersection between the flamelet and the laser illumination plane is determined. Tangents to these curves are tangents to the flamelet surface, and where flamelet curves in the two illumination planes intersect, the normal is obtained from the cross product of the intersecting tangent lines. Flamelet data obtained with the method are used to determine probability density functions of normals, flamelet crossing densities, flamelet surface densities, and estimates of the burning rate integral.

In addition, two-component laser Doppler velocimetry has been combined with compensated fine-wire thermocouple thermometry to obtain mass flux data required for calculating the burning rate integral. Measurements have been made on several methane-air V-flames, and the results demonstrate the utility of the method and the potential for turbulent burning velocity data to over estimate the acceleration of combustion by turbulence. Finally, the performance of ionization probes in premixed turbulent flame studies was evaluated.

I. MANUSCRIPTS

The following three manuscripts have appeared or been accepted for publication:

Gouldin, F. C., Combustion Intensity and Burning Rate of Premixed Flames, pp. 381 - 388 in the **Twenty-Sixth Symposium (International) on Combustion**, Combustion Institute, 1996.

Bingham, D. C., Gouldin, F. C. and Knaus, D. A., Crossed-Plane Laser Tomography: Direct Measurement of Flamelet Normal and Surface Density, to appear in the **Twenty-Seventh Symposium (International) on Combustion**, August 1998.

Ghenai, C., Gouldin, F. C. and Gokalp, I., Experimental Determination of the Burning Rate in Turbulent Premixed V-Flames using Simultaneous Velocity and Temperature Measurements, to appear in the **Twenty-Seventh Symposium (International) on Combustion**, August 1998.

The following paper has appeared as an AIAA preprint:

Gagnepain, L., Gouldin, F. C. and Gökalp, I., Evaluation of Uncooled Ionization Probes for Measurements in Premixed Turbulent Flames, **AIAA 96 - 0466**, presented at the 34th Aerospace Sciences Meeting, Reno Nevada, January, 1996.

The following has been submitted to a special issue of **Comb. Sci. and Technology**:

Knaus, D. A., Gouldin, F. C. and Bingham, D. C.: Assessment of Crossed-Plane Tomography for Flamelet Surface Normal Measurements.

In preparation:

One or two manuscripts will be submitted reporting flamelet normal measurements in spark ignition engines.

II. SCIENTIFIC PERSONNEL & DEGREES GRANTED

The following students were supported wholly or in part on the Grant:
Don Bingham, MS, Mechanical Engineering
Darin Knaus, MS/PhD, Mechanical Engineering
Dan Rog, MS, Mechanical Engineering

Dr. Chaouki Ghenaï was a visiting scientist working on the Grant.
Mr. Laurent Gagnepain was also a visiting scientist who worked on the grant.

The following graduate degree was awarded to a students:
Dan Rog, M. S. Mechanical Engineering,
"One Point and Two Point Statistics of Temperature Measurements in Premixed Wrinkled Laminar V Flames", Jan. 1997.
Donald C. Bingham, M. S. Mechanical Engineering,
"Crossed-Plane Tomography: Direct Measurement of Flamelet Orientation and Mean Flamelet Surface Density", Jan. 1998
Darin Kanus is working towards a PhD, expected data is January 2001.

III. INVENTIONS

NONE

IV. SCIENTIFIC ACCOMPLISHMENTS

Introduction

Premixed turbulent flames occur in a variety of different combustion systems including spark ignition engines and premixed prevaporized gas turbine combustors. For a range of conditions, chemical reactions in these flames are confined to thin sheets, flamelets, that separate regions of cold reactants from regions of hot products, the flamelet regime. The effects of flow turbulence in this regime are to wrinkle flamelets and to perturb the structure of the local reaction zone, affecting local gradients of temperature and composition within the flamelet sheet. It can be shown for such flames that the mean rate of product formation per unit volume is the product of the mean rate of product formation per unit flamelet area, $\langle B_L \rangle$ the mean perturbed laminar flame burning rate integral, and the mean flamelet surface area per unit volume, Σ the mean surface density.

$$\langle w \rangle = \langle B_L \rangle \Sigma. \qquad (1)$$

Turbulence intensifies combustion by increasing the mass of chemically reacting fluid per unit volume and in the flamelet regime Σ is the primary measure of this increase.

Traditionally, the turbulent burning velocity, u_T, has been used as the measure of the overall mean combustion rate in a premixed flame. While u_T data have been reported by many investigators, its definition, which is a generalization of that used for planar laminar flames, is ambiguous. In previous work, we have suggested that the burning rate integral, B_T, be used instead of u_T to quantify combustion rates in premixed turbulent flames. B_T is defined as the line integral of $\langle w \rangle$ along a line locally perpendicular to mean progress variable, $\langle c \rangle$, constant surfaces. This definition is unambiguous and reduces to the burning velocity times the reactant density in the planar flame limit.

In our ARO grant supported work, we have developed a method to measure directly for the first time the instantaneous orientation of a wrinkled flamelet and used the resulting data to find Σ. In addition, we have developed and tested a method for measuring B_T based on simultaneous velocity and temperature measurements. These developments have been reported in several papers and are summarized in this report.

Crossed-Plane Imaging for Measurement of Instantaneous Flamelet Surface Normal

Measurements of the surface normal, $\underline{N}$, have long been sought. Probability density functions of the normal quantify the degree and character of the flamelet wrinkling by turbulence. Gouldin [1] has shown that Σ can be related to the $\underline{N}$ distribution as follows:

$$\Sigma = \left\langle \frac{1}{|\underline{N} \bullet \underline{n}_y|} \right\rangle_c n_{cy}. \qquad (2)$$

$\underline{N}$ is the surface normal; the unit reactor $\underline{n}_y$ defines a direction in space and n_{cy}, the crossing density, is the average number of flamelet crossings per unit length of a line parallel to $\underline{n}_y$. The average denoted by $\langle \quad \rangle_c$ in Equation 2 is the crossing weighted average. In the literature there are several reports of $\underline{N}$ data, but all are essentially two-dimensional measurements. Only the Cornell measurements are fully three-dimensional, instantaneous flamelet surface normal measurements.

In planar imaging of a premixed flame by laser tomography, the reactant flow is seeded with a high vapor pressure oil mist which evaporates and reacts within the flamelet. The beam of a pulsed laser is formed into a sheet, and light scattered by the mist is recorded by a camera. The camera image contains bright regions of scattering from reactants and dark regions of products containing no mist. The boundaries between these regions correspond to where flamelets separating reactants from products intersect the laser illumination plane at the instant the laser is fired. Any line tangent to a boundary line revealed in an image is tangent to the flamelet surface.

For normal measurement, a second laser illumination plane is added, oriented perpendicular to the first plane. Two cameras simultaneously record images of scattering from each plane, and these images are processed to obtain the lines separating bright and dark regions in the image. The two laser illumination planes intersect and the corresponding line of intersection can be identified in each image. At points where the flamelet crosses the line of intersect in each image pair, tangents to the flamelet can be determined from the pair of camera images. In turn, the cross product of tangent pairs defines the flamelet normal at the instant the images are recorded and at the points where the flamelets cross the line of intersection between the laser illumination planes.

Along the line of intersection in each image, scattered light from both illumination planes is observed, and the light from the perpendicular or edge-on plane obscures light

from the other, or primary plane and making it difficult to find the flamelet boundary line in the image. Scattering from the edge beam is reduced by keeping the laser beam polarization within the illumination plane and placing a polarizer in front of the cameras.

To date, we have made crossed-plane tomography measurements of $\underline{N}$ in turbulent V-flames and a perturbed V-flame. The latter measurements we used to evaluate the accuracy of the method. In addition, Darin Knaus visited Sandia National Laboratories in August 1998 to make $\underline{N}$ measurements within a research, spark ignition. For these experiments the reactants were seeded with acetone, and the tripled output of a pulsed Nd:Yag laser was used for planar laser induced fluorescence (PLIF). Acetone is destroyed within flamelets, and therefore laser induced fluorescence marks regions of reactants in a way analogous to laser tomography. To suppress interference due to fluorescence from the edge-on illumination plane, a delay path is used to delay in time illumination in one plane from that in the other. Then the intensified CCD cameras used to acquire images are gated accordingly.

Cross-Plane Imaging Results

Evaluation of Method. As noted a technique, crossed-plane laser tomography, has been developed for the direct measurement of the instantaneous flamelet surface normal vector in turbulent premixed flames from two simultaneously acquired, orthogonal laser tomographic images. The method has been validated [2] through measurements made on a laminar V-flame, perturbed by a von Karman vortex street formed by a cylindrical rod placed in the reactant flow upstream of the flame and parallel to the flame stabilizing rod. Since the flame perturbations are two-dimensional, the flamelet normal can be measured by both crossed-plane tomography and single-plane tomography wherein the single plane is aligned perpendicular to the axis of the rod generating the Karman vortex street.

Comparison of the normals obtained in the two different ways reveals very good results. A scatter plot, Figure 1, of instantaneous flamelet normals measured by crossed-plane tomography shows that most normals fall in or very near to the vertical plane as expected, with larger deviations seen for normals that are nearly perpendicular to the line of intersection between the two illumination planes. A quantitative comparison of single plane and crossed-plane measurements is presented in Figure 2, where β is the angle of

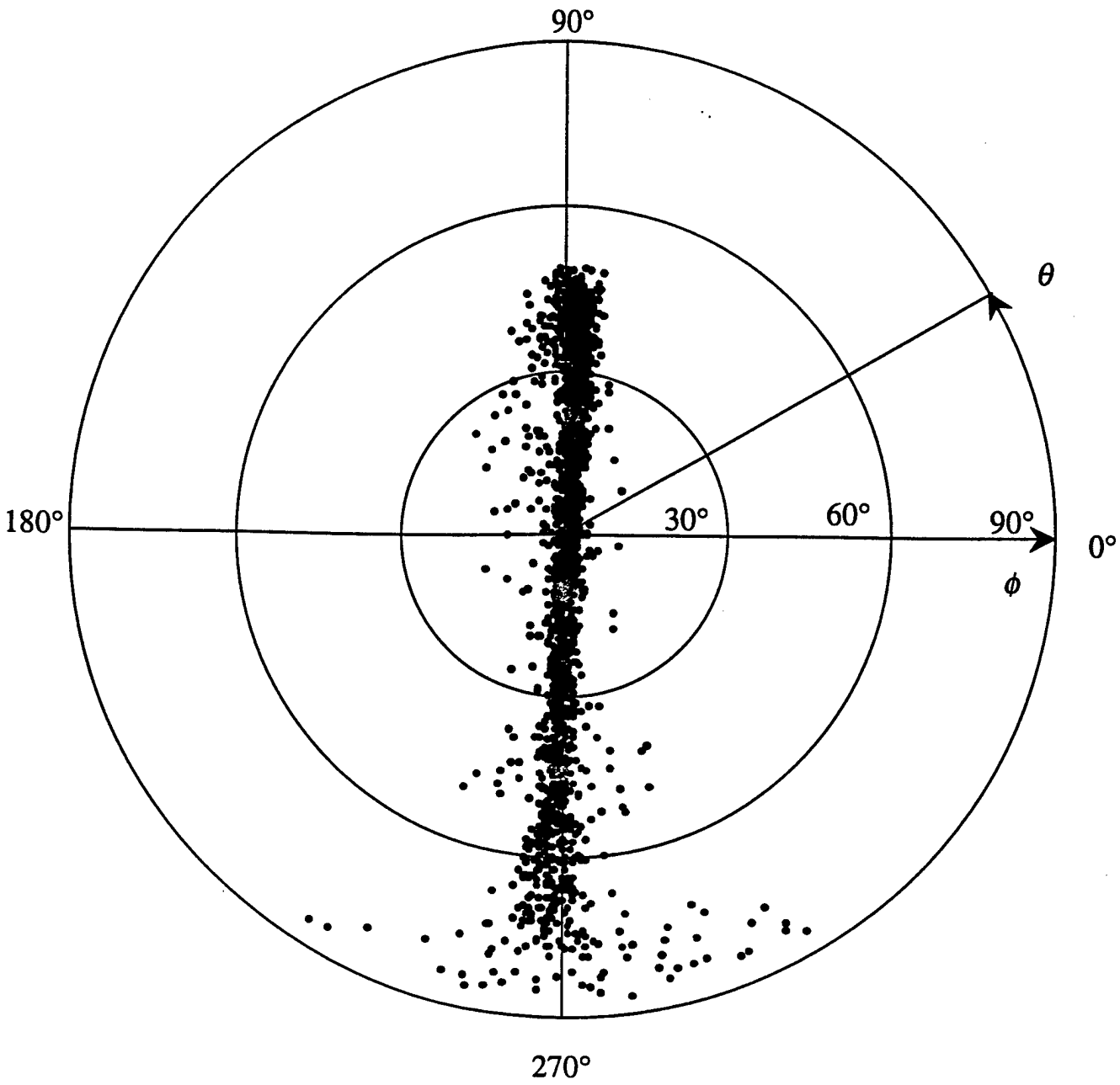

Figure 1. Polar plot of N measured via crossed-plane tomography in the perturbed laminar V-flame. The polar axis is the line of intersection between the two laser illumination sheets. ϕ is the polar angle; θ the azimuthal angle.

the projection of the normal onto the vertical plane and $P(\beta)$ is its probability density function (pdf). It can be seen in Figure 2 that the pdf's from the two methods are, within statistical uncertainty[1], nearly identical. The pdf of the angle between the surface normal measured using crossed-plane tomography and a vertical plane perpendicular to the stabilizing rod is nearly a delta function as expected, Figure 3; the standard deviation of this angle is only 3.7°, consistent with the flame's two-dimensional structure.

From an error analysis of uncertainty in the crossed-plane measurements of $\underline{N}$, it is concluded that uncertainty in the measurements caused by electronic noise and the discrete nature of the oil droplets is small, except for $\phi \rightarrow 0°$ and $\phi \rightarrow 90°$ where ϕ is the angle between $\underline{N}$ and the line of intersection. Estimated uncertainties in ϕ and in θ, the angle of rotation of $\underline{N}$ about the line of intersection versus ϕ are shown in Figure 4. Systematic errors in the technique have also been considered, and it is concluded that the accuracy of the validation measurements demonstrate that systematic error can be controlled by careful attention to laser alignment, suppression of light from the edge-on beam and appropriate image analysis.

Measurements on turbulent V-flames Crossed-plane tomography measurements have been performed on three turbulent flames at two streamwise locations in each flame, thereby generating six data sets for $\underline{N}$ with u'/u_L (the ratio of turbulent intensity to unstrained laminar burning velocity) varying between 0.64 and 1.72, Table 1 [3]. $\underline{N}$ values in each data set are expressed in polar coordinates (ϕ, θ), where ϕ is the polar angle, θ the azimuthal angle, and the polar axis is parallel to the mean of $\underline{N}$, $\langle\underline{N}\rangle$. The measurement results can be presented in terms of the joint pdf of ϕ and θ and related marginal pdf's, but first the distinction between the surfaced weighted joint pdf, $P_s(\phi, \theta)$ and the crossing weighted joint pdf, $P_c(\phi, \theta)$ must be drawn.

We define P_s such that $P_s(\phi, \theta) \sin\phi \, d\phi \, d\theta$ is proportional to the average fraction of the flamelet surface area within a unit volume with surfaces normals contained within

[1] Due to sample size neither curve is smooth.

Table 1: Flame Conditions and Summary of Results

Flame	Y (mm)	u (m/s)	u'/u_L	u_L (m/s)	ϕ	Fit Parameter σ (°)	$B_T/\rho_r u_L$ [a]	$B_T/\rho_r u_L$ [b]	<N> Orientation α angle (°)
Laminar	40	1.4	—	0.23	0.73	—	1.23	—	12
Turbulent 1	30	2.01	0.643	0.21	0.70	15.4	1.04	1.01	12
	80	2.47	0.685	0.21	0.70	25.5	1.15	0.97	6
Turbulent 2	80	4.30	0.956	0.21	0.70	37.7	1.30	1.15	7
	40	4.21	1.023	0.21	0.70	25.7	1.16	1.39	12
Turbulent 3	40	6.46	1.650	0.23	0.72	29.3	1.18	1.45	10
	80	6.42	1.732	0.23	0.72	39.5	1.32	1.43	5

[a] Bingham, et al. [b] Ghenai, et al.

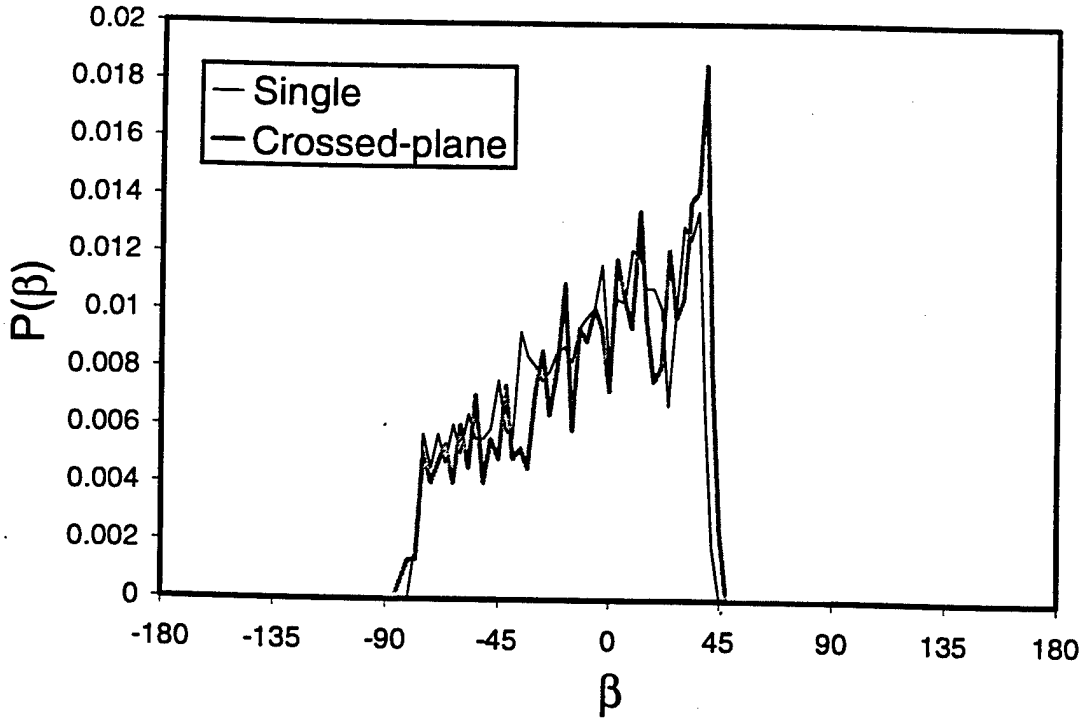

Figure 2. Comparison of pdf's of β measured via crossed-plane tomography.

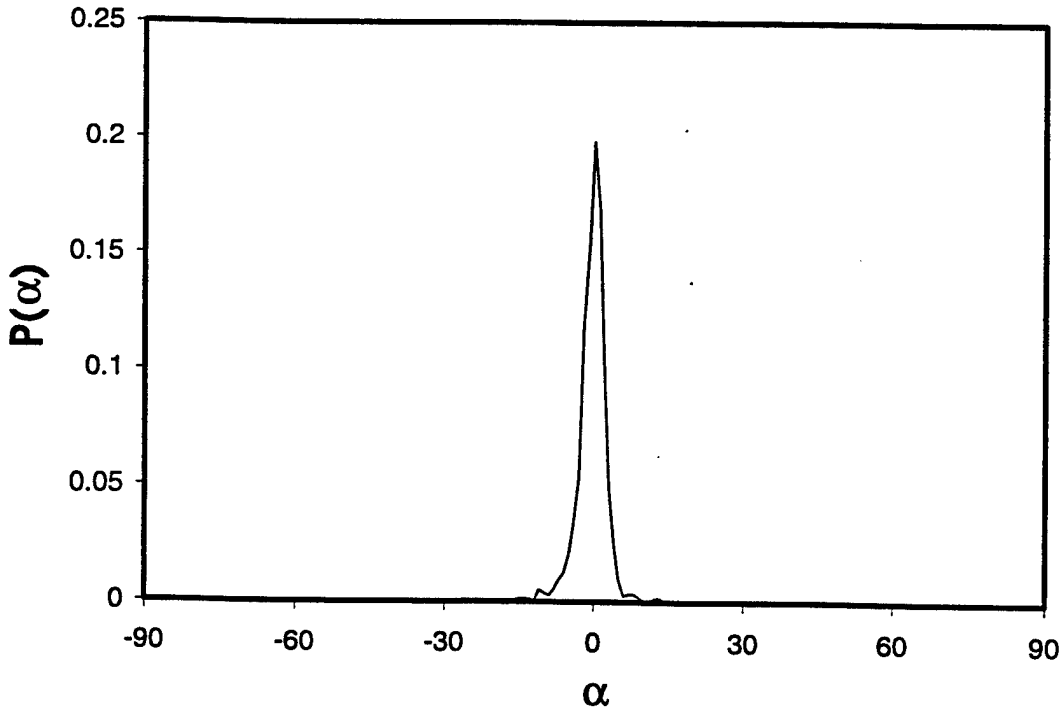

Figure 3. Pdf of α measured using crossed-plane tomography.

the differential solid angle, $d\Omega(\phi, \theta) = \sin\phi\, d\phi\, d\theta$. To define P_c, consider a small right cylinder with its axis parallel to the unit vector $\underline{n}_y$. Then $P_c\, d\Omega$ is the fraction of all flamelet elements crossing the axis of the cylinder that cross with a normal vector within the solid angle $d\Omega$ [2]. These two pdf's are related, it can be shown, as follows: $P_c\, d\Omega = A\, |\underline{N} \bullet \underline{n}_y|\, P_s\, d\Omega$, where A is a normalization constant. Finally, we note that crossed-plane tomography measurements give crossing weighted results, and therefore, pdf's extracted from these data are crossing weighted.

In Figures 5 a and b marginal pdf's of ϕ and θ obtained from $P_c d\Omega$ are shown for one of the six data sets. Shown also in the Figure 5 b is a fit of the marginal pdf obtained from a $P_c d\Omega$ of the form $A|\underline{N} \bullet \underline{n}_y| \exp(-(\phi/\sigma)^2 \sin\phi\, d\phi\, d\theta$, which is consistent with a surface weighted joint pdf of ϕ and θ of the form $P_s(\phi,\theta) = C \exp(-(\phi/\sigma)^2)$, a single parameter function, independent of θ. The fit parameter, σ, is found to increase with turbulence intensity and distance from the stabilizing rod. This finding is potentially very significant if P_s for other flame configurations takes the same, single parameter form. For example, it follows that Σ is in this case a universal function of σ and n_{cy}, the crossing density along $\underline{n}_y$, with $\underline{n}_y = \langle\underline{N}\rangle$ for all flames. Furthermore, by integration it can be shown that the direction cosine term, $\langle 1/|\underline{N} \bullet \underline{n}_y|\rangle_c$, is a monotonic function of σ increasing smoothly from 1 to its maximum value of 2. Hence large values of Σ result from large values of the crossing density n_{cy}.

For each data set the mean inverse direction cosine can be evaluated, and the burning rate integral scaled by the product of the reactant gas density and the unstrained laminar burning velocity, $B_T/\rho_r u_L$, estimated under the assumption that I_o is one. (See below for a discussion of B_T.) For both quantities the values obtained are near one and increase with increasing turbulence and distance downstream from the stabilizing rod. The low values of the direction cosine are physically reasonable but, it must be noted, do not agree with previous estimates made with single plane image data (e.g., Chew, Bray, and Britter [4] and Santavicca, et al [5]). The difference is attributed to the error incurred

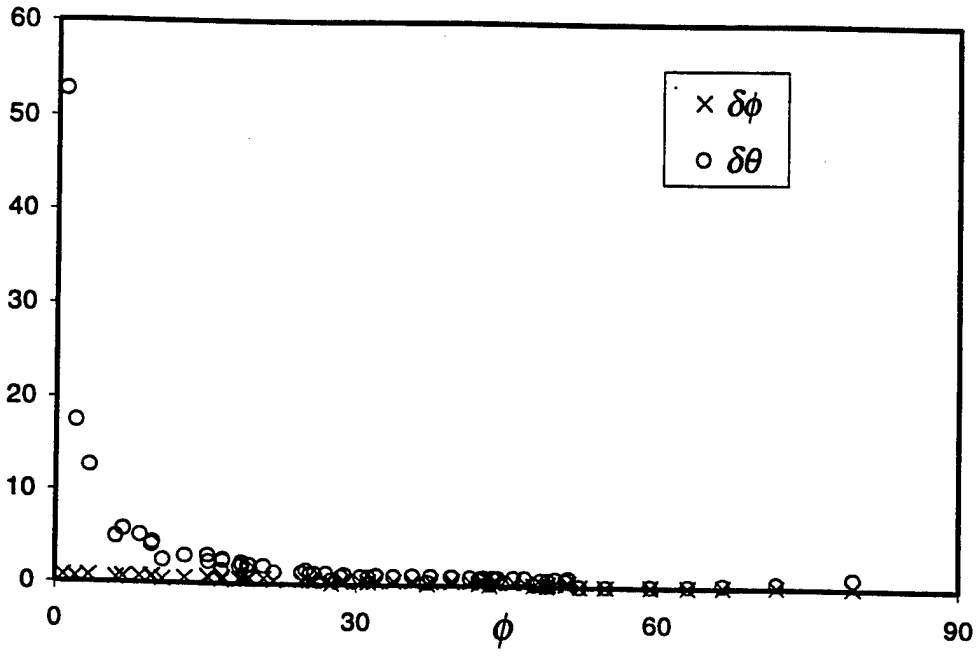

Figure 4. Uncertainty in the measurement of ϕ and θ evaluated on a test image.

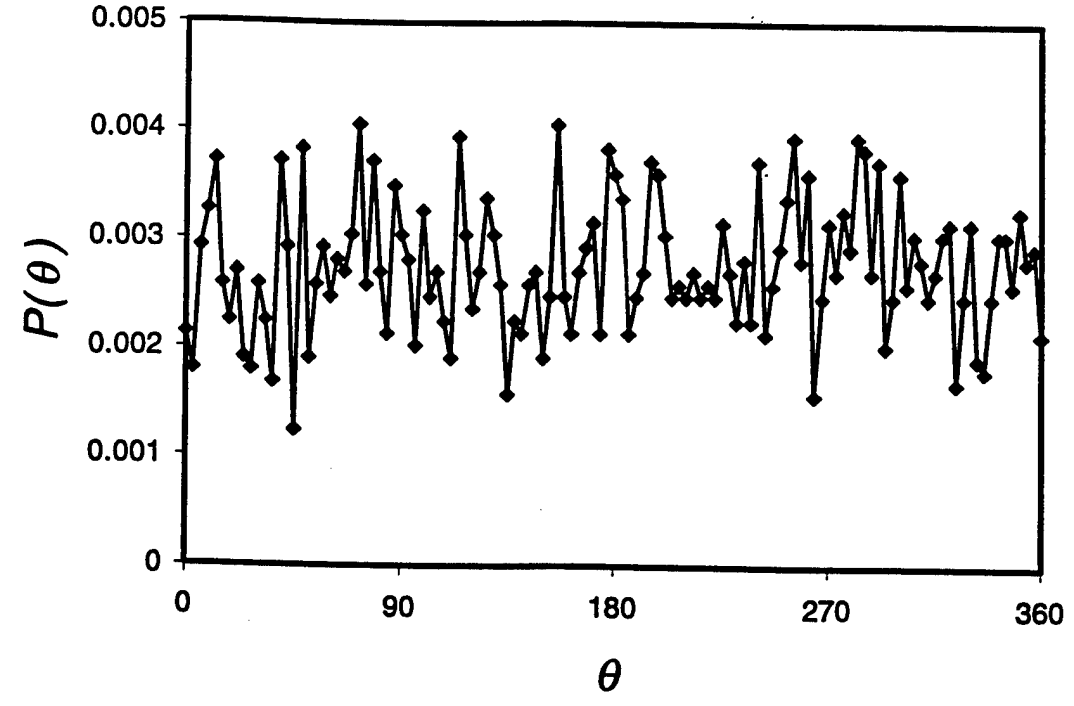

(a)

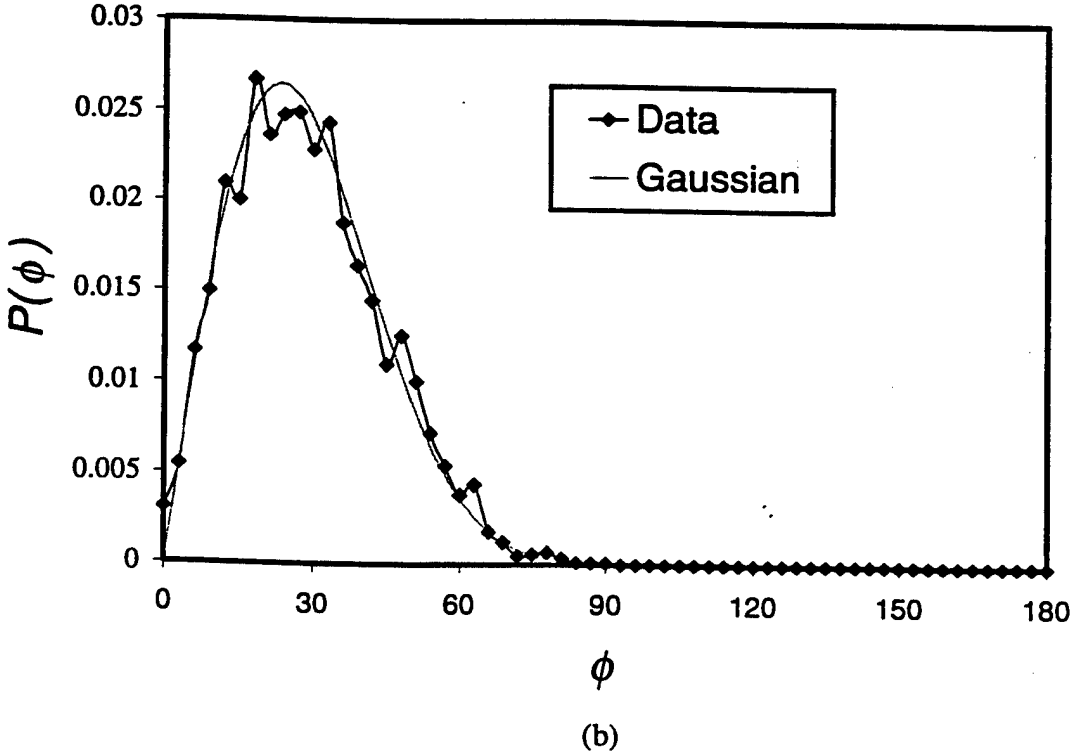

(b)

Figure 5. Crossing-weighted marginal pdf's of a) ϕ and b) θ in turbulent flame number 2. The smooth curve in b) is the curve fit discussed in the text.

in using two-dimensional data to estimate the normal. The burning rate integral estimates can be compared with independent evaluations of $B_T/\rho_r u_L$ based on simultaneous measurements of velocity and density made on the same flames, Figure 6 (see also below). With the exception of the most turbulent flame, the comparison between the two data sets are very good and give support to the validity of both measurement methods. The $B_T/\rho_r u_L$ value estimated at the highest turbulence level studied is low, and the difference is attributed to an underestimate of N_c, the integral of n_{cy} cross the flame brush. Based on the results cited, it is concluded that crossed-plane tomography can be used with confidence to measure flamelet surface normals and crossing densities along the line of intersection of the laser illumination planes in laboratory burners.

Measurements in a Spark Ignition Engine [6]. In August 1998, Darin Knaus visited Sandia National Laboratories in Livermore, CA and worked with Paul Hinze and Paul Miles to test the use of crossed-plane imaging in a research engine having good optical access. The goals of this work were to demonstrate the feasibility of measuring flamelet surface normals in spark ignition engines, obtain normal data, and compare these data to data from V-flames.

For these measurements, acetone planar laser induced fluorescence (PLIF) replaced laser tomography as the imaging method, and to suppress interference from the edge-on beam an optical delay loop was used to separate in time illumination in the two, crossed planes. The laser source was the tripled output of a pulsed Nd:Yag laser, while gated, intensified CCD cameras recorded the fluorescence images. Since acetone is destroyed within a flamelet, the PLIF images are analogous to those obtained by laser tomography. Consequently, image pairs were analyzed in the same way that laser tomography images were analyzed.

Measurements were made with two different optical configurations and three different engine operating conditions for a total six different data sets. Three of these sets have been analyzed and work continues on the others. From pairs of images we have been successful in determining surface normals and pdf's, and also have been able to determine lines of constant mean progress variable and in turn the normals to mean

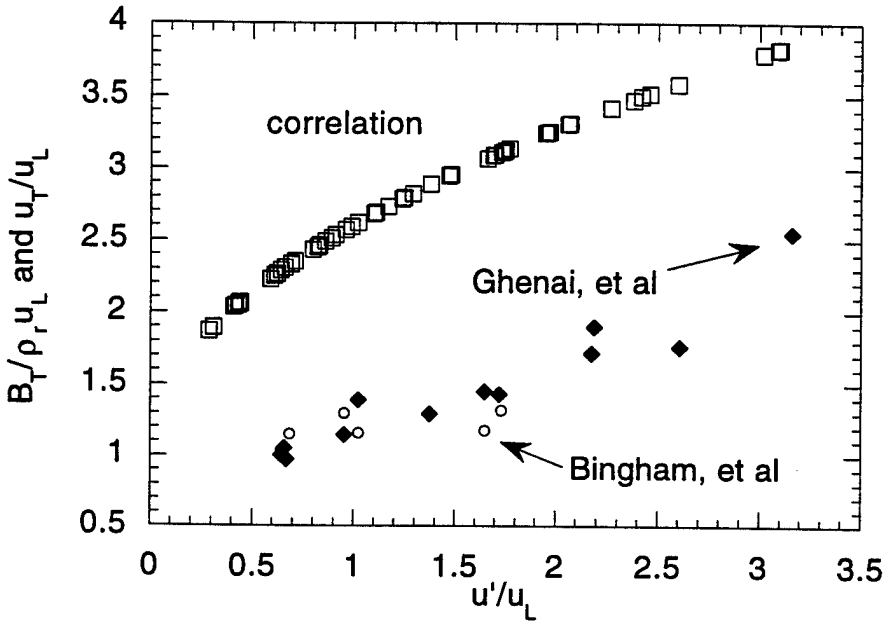

Figure 6. Burning rate integral data scaled by the mass flux per unit area across the corresponding unstrained laminar flame obtained 1) by simultaneous velocimetry and temperature measurements (Ghenai, et al), 2) from flamelet normal data (Bingham, et al) and 3) a correlation dur to Gulder [16].

progress variable constant surfaces along the line of intersection between the two laser illumination planes. For example, in Figure 7 marginal pdf's of ϕ and θ are presented and compared to fits obtained from a joint pdf of the form $A|\underline{N} \bullet \underline{n}_y| \exp(\phi^2/\sigma^2) \sin\phi \, d\phi \, d\theta$, $\sigma = 75°$. $\underline{n}_y$ denotes the orientation of the line of intersection between the two laser illumination planes, and as above the polar axis is defined by $<\underline{N}>$, the mean surface normal. A similar fit was found to be satisfactory for V-flame data, but is not entirely satisfactory for engine data. This is especially true for the marginal pdf of θ which has an unexpected peak at $\theta = 0°$.

Future plans include measurements on higher turbulence level flames than those studied to date to test the PDF fit and allow empirical information to be gathered on the nature of the PDF and of n_{cy}. Measurements are planned on different flame geometry's, particularly on a stagnation plate burner with axial symmetry. The effect of stable and unstable preferential diffusion conditions on $\underline{N}$ distributions will be studied. Improving data rates will allow larger data sets to be compiled, and variations in statistics with $<c>$ across the flame brush will then be studied.

Burning Rate Integral Determination

As noted, it has been traditional to use the turbulent burning velocity as the measure of the integrated combustion rate in premixed turbulent flames in spite of the fact that this quantity is ill-defined in all but normal turbulent flames [7]. Recently, several researchers have suggested replacing, as a measure of the overall combustion rate, the ill-defined turbulent burning velocity with the well-defined turbulent burning rate integral [7 - 9] which, in turn, is the integral of $<w>$ along a line y perpendicular to mean progress variable, $<c>$, constant contours and spanning the turbulent flame brush.

$$B_T = \rho_r u_L \int_{-\infty}^{\infty} <w> \, dy \qquad (3)$$

Furthermore, Gouldin [1] has shown that in most cases

$$B_T = \rho_r u_L \int_{-\infty}^{\infty} I_o < \frac{1}{|\underline{N} \bullet \underline{n}_y|} >_c n_{cy} \, dy$$

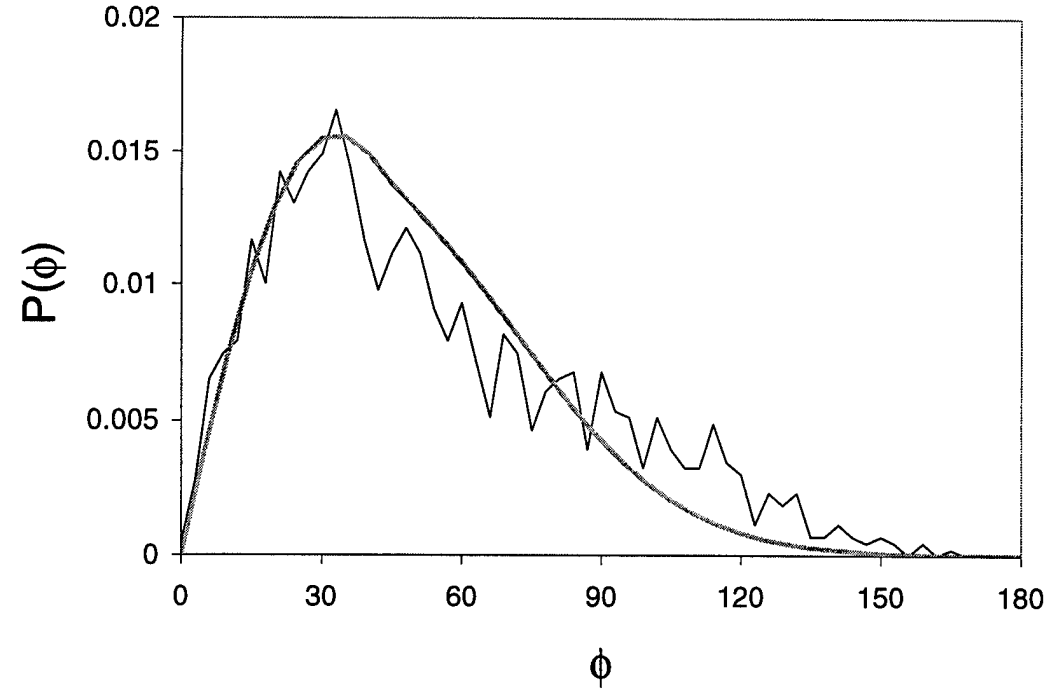

(a)

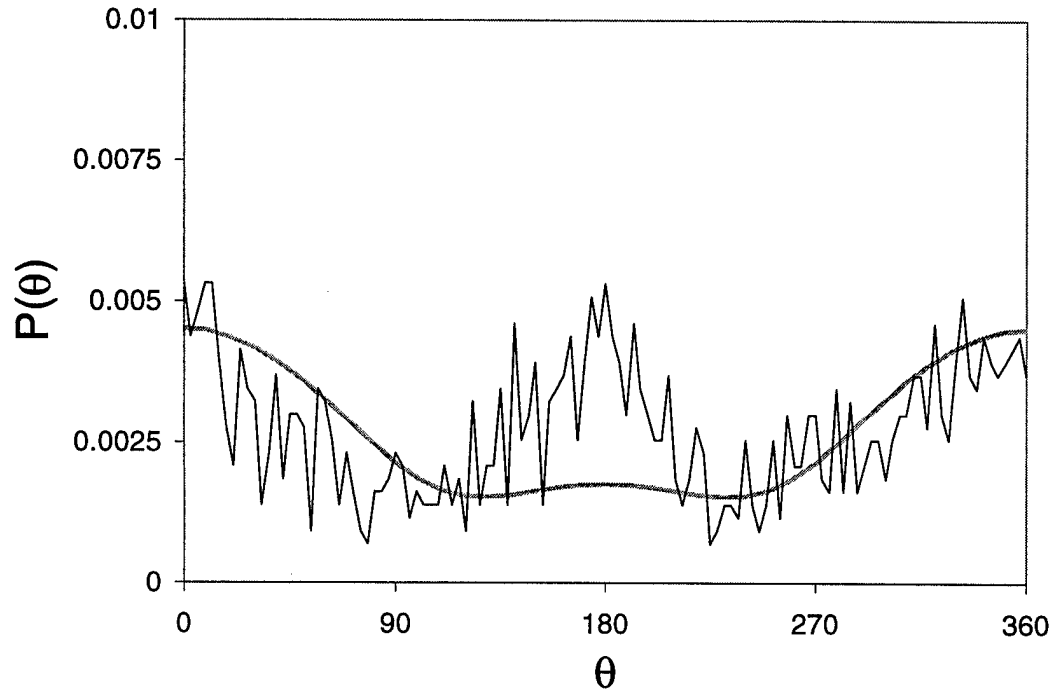

(b)

Figure 7. Marginal PDF's of ϕ and θ for the 600 RPM engine speed. The crossing-weighted, joint PDF is fit by
$P_c(\phi,\theta) \sin\phi \, d\phi d\theta = A \, |\underline{N} \bullet \underline{n}_\eta| \exp(-\phi^2/\sigma^2) \sin\phi \, d\phi \, d\theta$.

$$= \rho_r u_L < I_o < \frac{1}{|\underline{N} \cdot \underline{n}_y|} >_c >_{cF} N_c, \qquad (3)$$

where $\int_{-\infty}^{\infty} n_{cy}\, d_y = N_c$ and cF denotes a crossing weighted average along y over the flame brush. I_0 accounts for flamelet structure perturbation effects on the burning rate integral, and $<B_L> = I_0\, \rho_r\, u_L$. It is important to note that, while $\underline{n}_y$ in Eq. (2) is arbitrary, in order to obtain Eq. (4), $\underline{n}_y$ must be perpendicular to <c> contours. This is an important distinction to make since this direction is perpendicular to the one adopted by Bray, Moss and Libby [10] in their crossing density, closure model. In the previous section, $B_T / \rho_r\, u_L$ was estimated from flamelet normal data with Eq. (4) and $I_0 = 1$. Below is discussed a method for finding B_T from velocity and temperature data [11].

While B_T is well defined, it is an integral quantity and challenging to measure [7, 8]. We have developed and demonstrated a method for measuring the burning rate integral in turbulent premixed flames and have reported data obtained from several V-flames via the method [11]. A relationship for B_T in terms of integrals of convective and turbulent fluxes of progress variable can be obtained from the governing equation for <c>. In turn, B_T is obtained from data for mass fluxes normal and tangent to Favre mean progress variable constant surfaces that are integrated across the turbulent flame brush.

The determination of both convective and turbulent mass fluxes is made by simultaneous, two component velocity (axial and lateral) and temperature measurements using a combination of two-component LDV and a compensated, fine-wire thermocouple, where the instantaneous gas density is obtained from the instantaneous temperature through the equation of state and the assumption of constant pressure. The time constants required for thermocouple compensation are obtained by a method developed and tested in our laboratory under ARO support [12, 13, 14].

So far B_T data for lean CH_4 - air flames, for ratios of turbulence intensity to laminar burning velocity between 0.643 to 3.16, have been obtained. These data demonstrate the utility of simultaneous velocity and temperature measurements for burning rate integral determination in laboratory burners. They further show 1) that conditional velocity data alone can not be used with confidence to estimate mass fluxes in the flamelet regime, 2) that the use of velocity data from the reactant side of the turbulent flame brush to estimate B_T (or the turbulent burning velocity) results in estimates that are quite high, 3) that B_T is a strong

function of u'/u_L. For design purposes, B_T is the most important quantity to be able to predict.

$B_T / \rho_r u_L$ data obtained by temperature and velocity data are compared in Figure 6 to estimates of this quantity from normal data. The results are very good and support the validity of both measurements. Shown also in Fig. 6 are estimates of the same quantity based on a widely used correlation for the turbulent burning velocity (u_T / u_L). These estimates are very high, indicating that u_T data can not be trusted to quantify the overall impact of turbulent on mean combustion rates.

Ionization Probe Evaluation

Early in the grant period we performed an evaluation of ionization probes for the measurement of flamelet crossing events and of $\underline{N}$ [16]. Ionization probes have been used extensively by Japanese investigators for flamelet crossing event determination. These probes are simple to make and use, but the interpretation of the recorded signals can be ambiguous. In our evaluation using a laminar Bunsen flame and a perturbed laminar V-flame, we find that the determination of crossing events with an ionization probe can be quite uncertain and that for many flame conditions these probes are unsuitable for use.

Summary and Conclusions

The development of a new technique, crossed-plane tomography, and its application to measure, for the first time, instantaneous flamelet surface normals in several premixed, turbulent flames is reported. The normal is calculated from data extracted from tomographic images recorded simultaneously with CCD cameras from two orthogonal laser illumination planes. In each image, the locus of flamelet locations is determined, and **N** is obtained by taking the cross produced of the tangents to these loci at their point of intersection. To test the new technique a series of measurements were performed on a perturbed laminar flame, and the results demonstrate the validity of the technique.

In future studies, we plan to apply our technique to different burners and fuel-air combinations for a broad range of turbulence levels. A focus will be on the variation of the direction cosine term and N_c with turbulence level. It is expected that these two

quantities are related and that the cosine term will first increase from one, then peak and finally asymptote to 2 as turbulence increases [1]. Of great interest is its value at the peak. If the surface weighted joint pdf form is found to be independent of turbulence level, we already know from calculation that the peak value is only slightly above 2.

Finally, we note that there are obvious extensions of the crossed-plane technique including crossed-plane Rayleigh and florescence imaging. In principle, any planar imaging technique that yields instantaneous iso-contours could be used in crossed-plane imaging to obtain along the line of intersection of the two illumination planes iso-scalar surface normals and scalar gradients.

B_T measurements need to be continued to build a data base. Our results to date indicate that turbulent burning velocity date can substantially over measure the influence of turbulence on combustion rates. Since burning velocity data are frequently used to test model predictions it is important that B_T measurements be continued in order to replace missing burning velocity data with well defined B_T data.

V. REFERENCES

1. Gouldin, F. C.: Analysis of Certain Closure Models for Premixed Turbulent Combustion, pp. 433 - 459 in **Physical and Chemical Aspects of Combustion: A Tribute to Irvin Glassman**, R. F. Sawyer and F. L. Dryer, edts., Gordon and Breach Science Publishers, Amsterdam, 1997.

2. Knaus, D. A., Gouldin, F. C. and Bingham, D. C.: Assessment of Crossed-Plane Tomography for Flamelet Surface Normal Measurements, submitted to **Comb. Sci. Tech.**

3. Bingham, D. C., Gouldin, F. C. and Knaus, D. A., Crossed-Plane Laser Tomography: Direct Measurement of Flamelet Normal and Surface Density, to appear in the **Twenty-Seventh Symposium (International) on Combustion**, The Combustion Institute, Pittsburgh, 1998.

4. Chew, T. C., Bray, K. N. C. and Britter, R. E., **Comb Flame 80**, 65, 1990.

5. Lee, T. - W., North, G. L. and Santavicca, D. A., **Comb. Sci. Technol. 84**, 121, 1992.

6. Knaus, D. A., Gouldin, F. C., Hinze, P. C. and Miles, P. C.: Measurements of Flamelet Surface Normal in an Optical SI engine by Crossed-Plane Imaging, to be presented at the Joint Meeting of the United States Sections of the Combustion Institute, GWU, Washington, D. C., March 15-17, 1999.

7. Gouldin, F. C.: **Twenty - Sixth Symposium (International) on Combustion**, 381 - 388, 1996.

8. Bourguignon E., Kostiuk L.W., Michou Y. and Gokalp I.: **Twenty-Sixth Symposium (International) on Combustion,** 447- 453, 1996.

9. Shepherd I.G. and Kostiuk L.W.: **Combust. Flame 96**, 371-380,1994.

10. Bray, K. N. C., Libby, P. A. and Moss, J. B.: **Twentieth Symposium (International) on Combustion**, 421-427, 1984.

11. Ghenai, C., Gouldin, F. C. and Gokalp, I., Experimental Determination of the Burning Rate in Turbulent Premixed V-Flames using Simultaneous Velocity and Temperature Measurements, to appear in the **Twenty-Seventh Symposium (International) on Combustion**, The Combustion Institute, Pittsburgh, 1998.

12. Miles, P. C. and Gouldin, F. C., **Combust. Sci. Tech. 89**, 181-199, 1993.

13. Tache, M. M. and Gouldin, F. C., Evaluation of Compensated Thermocouple Measurements in Premixed Flames, **AIAA 95-0142**, presented at the 33rd Aerospace Sciences Meeting, Reno Nevada, January 9-12, 1995.

14. Rog, D., "One Point and Two Point Statistics of Temperature Measurements in Premixed Wrinkled Laminar V Flames", M. S. Thesis, Cornell University, Ithaca, NY, January 1997.

15. Bingham, D. C., Crossed-Planer Tomography: Direct Measurement of Flamelet Orientation and Mean Flamelet Surface Density, M. S. Thesis, Cornell University, Ithaca, N. Y. 14853.

16. Gulder, O., pages 743 – 750 in the **Twenty-Third Symposium (International) on Combustion**, The Combustion Institute, Pittsburgh, 1998.

V. EXTERNAL INTERACTIONS

Presentations

The following presentations, on work supported by or directly related to ARO sponsored research, were made as noted:

Gouldin, F. C., Combustion Intensity and Burning Rate of Premixed Flames, pp. 381 - 388 in the **Twenty-Sixth Symposium (International) on Combustion**, Combustion Institute, 1996.

Gagnepain, L., Gouldin, F. C. and Gökalp, I., Evaluation of Uncooled Ionization Probes for Measurements in Premixed Turbulent Flames, **AIAA 96 - 0466**, presented at the 34th Aerospace Sciences Meeting, Reno Nevada, January, 1996.

C. Ghenai, F. C. Gouldin and I. Gokalp, Experimental Determination of the Burning Rate in Turbulent Premixed V-Flames using Simultaneous Velocity and Temperature Measurements, presented at the 1997 Fall Technical Meeting of the Eastern States Section of the Combustion Institute, October 27 - 29, 1997, Hartford, CT.

D. C. Bingham, F. C. Gouldin and D. A. Knaus, Crossed-Plane Laser Tomography: Direct Measurement of Flamelet Normal and Surface Density, presented at the 1997 Fall Technical Meeting of the Eastern States Section of the Combustion Institute, October 27 - 29, 1997, Hartford, CT.

Bingham, D. C., Gouldin, F. C. and Knaus, D. A., Crossed-Plane Laser Tomography: Direct Measurement of Flamelet Normal and Surface Density, presented at the **Twenty-Seventh Symposium (International) on Combustion**, The Combustion Institute, Pittsburgh, 1998.

Ghenai, C., Gouldin, F. C. and Gokalp, I., Experimental Determination of the Burning Rate in Turbulent Premixed V-Flames using Simultaneous Velocity and Temperature Measurements, presented at the **Twenty-Seventh Symposium (International) on Combustion**, The Combustion Institute, Pittsburgh, 1998.

Knaus, D. A., Gouldin, F. C., Hinze, P. C. and Miles, P. C.: Measurements of Flamelet Surface Normal in an Optical SI engine by Crossed-Plane Imaging, to be presented at the Joint Meeting of the United States Sections of the Combustion Institute, GWU, Washington, D. C., March 15-17, 1999.

Combustion Research Center Collaboration

We have been collaborating with Paul Miles and Paul Hinze at the Combustion Research Facility at Sandia National Laboratories, Livermore, CA. Darin Knaus visited there in August 1998 to obtained crossed-PLIF data in a research engine. The experiments went very well, and we continue to analyze the data Darin obtained with the help of Paul Hinze and Paul Miles.

International Collaboration

In addition to support from ARO we had a grant from NSF to support collaboration with Drs. Iskender Gökalp and Michel Champion of CNRS, France and Professor Ken Bray of Cambridge, UK. As part of that collaboration Dr. Chaouki Ghenaï and Laurent Gagnepain visited us and worked on burning rate measurements and the evaluation of ionization probes for flames measurements.

VI. APPENDIX

In support of the material in this report copies of the following are attached.

Knaus, D. A., Gouldin, F. C. and Bingham, D. C.: Assessment of Crossed-Plane Tomography for Flamelet Surface Normal Measurements, submitted to **Comb. Sci. Tech.**

Knaus, D. A., Gouldin, F. C., Hinze, P. C. and Miles, P. C.: Measurements of Flamelet Surface Normal in an Optical SI engine by Crossed-Plane Imaging, abstract of paper to be presented at the Joint Meeting of the United States Sections of the Combustion Institute, GWU, Washington, D. C., March 15-17, 1999.

Please note that the following will be available in the next few months.

C. Ghenai, F. C. Gouldin and I. Gokalp, Experimental Determination of the Burning Rate in Turbulent Premixed V-Flames using Simultaneous Velocity and Temperature Measurements, to appear in the **27th Symposium (International) on Combustion**

D. C. Bingham, F. C. Gouldin and D. A. Knaus, Crossed-Plane Laser Tomography: Direct Measurement of Flamelet Normal and Surface Density, to appear in the **27th Symposium (International) on Combustion**

Measurements of Flamelet Surface Normals in an Optical SI Engine by Crossed-Plane Imaging

D. A. KNAUS, F. C. GOULDIN. *Cornell University, Ithaca, NY. E-mail: fcg2@cornell.edu.*
P. C. HINZE and P. C. MILES. *Combustion Research Facility, Sandia National Laboratory, Livermore, CA*

Introduction

There is considerable interest in the topography of flamelet surfaces in premixed, turbulent flames due to the relationship between the wrinkling of the flamelet surface and the burning rate. The widely accepted equation [1] for the burning rate is:

$$\langle w \rangle = \rho_r u_L I_o \Sigma. \qquad (1)$$

Here, ρ_r is the reactant density; u_L is the unstretched laminar burning velocity; I_o is a factor that accounts for stretch effects on the laminar burning velocity; and Σ is the mean flamelet surface density. Σ depends on the degree of wrinkling of the flamelet surface. Gouldin [2] has derived a general expression relating Σ and the flamelet surface normal, **N**, distribution:

$$\Sigma = n_\eta \left\langle \frac{1}{|\sigma_n|} \right\rangle, \qquad (2)$$

where n_η is the spatial flamelet crossing density along a line η and σ_η is the direction cosine of **N** with respect to η. **N** is defined as a unit vector normal to the flamelet surface oriented in the direction of the flamelet propagation, i.e. into the reactants.

Laser tomography and PLIF are well established methods for imaging premixed turbulent flames[3,4]. Laser tomography involves introducing into the reactants seeding particles such as oil droplets which scatter light from an incident laser sheet. The seeding particles disappear in the flamelet via evaporation or burning, so that no light is scattered in the products. Images of scattering are recorded with the optical axis of the imaging device aligned normal to the laser illumination plane. The intersection of the flamelet with the laser sheet, the flamelet boundary, is determined in the images as the boundary between light reactant and dark product regions. Similar images can be measured by PLIF: the reactants are seeded with a species that fluoresces when excited by the incident laser sheet, and that is destroyed by chemical reaction in the flame. Statistical information about the wrinkling of the flamelet in the plane of the laser sheet can be determined from sets of these images.

The recently developed crossed-plane imaging technique allows information about the flamelet structure to be measured in three dimensions through simultaneous, orthogonal images. Two orthogonal laser sheets are incident on the flame, and **N** and n_η are measured along the line defined by the intersection of the two sheets, referred to as the measurement line. This technique has been previously applied to turbulent V-Flames [5], and the accuracy of the technique has been demonstrated [6,7]. The intention of the current work is to demonstrate the feasibility of the technique for flamelet surface normal measurements in an optically accessible internal combustion engine, to report **N** distributions in the form of PDF's, and to discuss briefly the characteristics of these PDF's.

Experimental Setup

Optical Engine

The measurements were made in a 4-valve, pent-roof optical engine based on a General Motors production engine. Optical access to the clearance volume is obtained through flat windows in the gables of the head, as well as through a Bowditch piston arrangement. The Bowditch piston arrangement allows visualization of the cylinder through a quartz window in the piston via a mirror in the extended piston, Fig. 1.

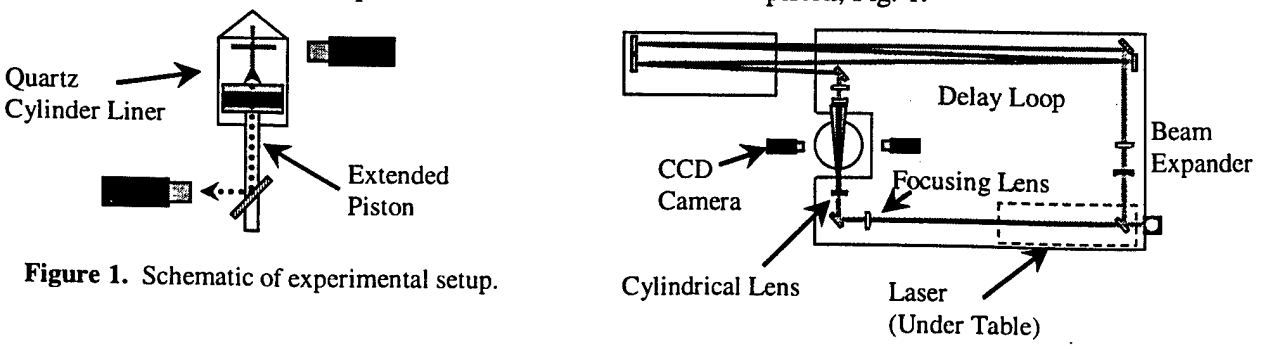

Figure 1. Schematic of experimental setup.

Additional access to the swept volume is obtained by use of a full quartz cylinder liner. The engine is characterized by a bore of 9.2 cm, a stroke of 8.5 cm, and a compression ratio of 9.5:1. The engine is fueled with premixed propane-air, which has been seeded with acetone to permit the acquisition of PLIF images. The propane and acetone are metered such that the overall charge equivalence ratio is 1.0, as determined by a lambda sensor in the exhaust. Acetone makes up approximately 20% of the total fuel load. Measurements were made at engine speeds of 600, 1200, and 1800 RPM. The spark timing was set at 9, 11, and 13° ATDC respectively so that the flame kernel would consistently intersect the measurement line.

Imaging System

PLIF images are obtained by exciting the acetone with 266 nm laser radiation generated by quadrupling the output of a pulsed Nd:YAG laser, and broadband collection of the resulting fluorescence using intensified CCD cameras. Two orthogonal laser sheets are formed via cylindrical lenses and propagated through the engine, such that the line of intersection of the two sheets lies in a horizontal plane and bisects the cylinder axis approximately 5 mm below the gasket plane, Fig. 1. The maximum sheet thickness within the cylinder is estimated to be less than 0.5 mm. One sheet is oriented vertically, and the other horizontally. Fluorescence from the vertically oriented laser sheet is imaged through the cylinder liner, while fluorescence from the horizontal laser sheet is imaged via the mirror in the extended piston.

To eliminate interference in the images due to fluorescence induced by the edge-on laser sheet, the arrival times of the laser sheets are separated by approximately 50 ns via an optical delay loop, and the intensifiers on the CCD cameras are gated correspondingly. The field of view of the camera imaging directly through the cylinder liner is 21x28 mm and the field of view of the camera imaging through the piston is 25x32 mm.

Image Processing

Approximately 1000 image pairs were acquired and saved for image processing at each engine speed. A pair of raw images can be seen in Figs. 2a and b. Fig. 2a shows the bottom view of the horizontal laser sheet, imaged through the piston. Fig. 2b shows the side view of the vertically oriented laser sheet, imaged through the cylinder liner. Because the cameras are positioned on opposite sides of the engine, features in the images appear rotated 180°, i.e. the left side of one image corresponds to the right side of the other. The dark area at the bottom of Fig 2b is the piston. The intake valves are located on the right side of Fig. 2a. The left side of Fig. 2b will be referred to as the front side of the kernel, and the right side as the back. The image resolution is greater than 0.2 mm.

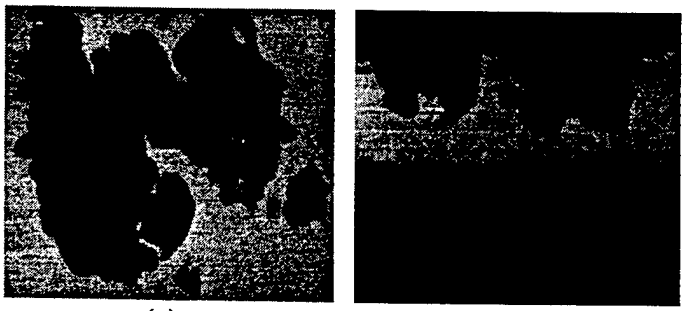

(a) (b)

Figure 2. Raw image pair. Image (a) is the bottom view through the piston. Image (b) is the side view.

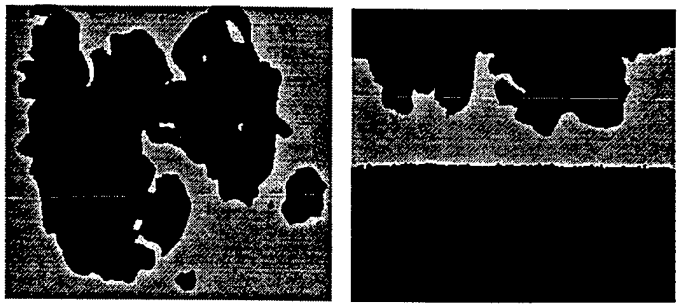

Figure 3. Same image pair after image processing.

Image processing begins with a thresholding step, making the images binary. Features smaller than approximately 0.2 mm are then removed through pixel erosion and dilation Flamelet crossings are identified along the measurement line in the two images. The location of the measurement line in the images is determined by switching the gating of the two cameras so that the cameras image fluorescence from the edge-on sheet. An image pair is acquired while the engine motors (without spark). The edge-on sheets appear as lines, and are linearly fit to define the location of the measurement line. Crossings are then identified in the two images. In some cases, due to uncertainty in the location of the measurement line, a flame feature that is recorded as a crossing in one image may not appear as a crossing in the other image; these crossings are discarded. The flamelet boundary is located for all registered crossings by an edge-finding algorithm. The boundary is parameterized and fit in parametric space by a second order polynomial, and the slope of the flamelet boundary where it crosses the measurement line is determined from the parametric fits. Figs. 3a and b show the same image pair as Figs. 2a and b after image processing. The slopes are used to define unit vectors tangent to the flamelet

boundary in each image. The cross product of these two tangent vectors is perpendicular to both vectors, and is therefore normal to the flamelet surface. The data obtained by imaging are grouped according to which side of the kernel the crossing occurs on. Normal vectors are assigned to either the front or the back side based on the location of the crossing along the measurement line: crossings measured to the left of center in Fig. 2b are assigned to the front side, crossings measured to the right of center are assigned to the back side.

Results and Discussion

For each data set, the mean flamelet surface normal, <N >, is determined, and each N's specification is transformed into polar coordinates in terms of a polar angle, ϕ, and an azimuthal angle, θ, with <N > as the polar axis. Table 1 presents measured values of <N>, n_η, as well as the total number of normals measured. The Cartesian coordinates used to describe <N> are oriented with z in the vertical direction, y along the line of intersection from the front side of the flame kernel to the back (left to right in Fig. 2b), and x in the horizontal plane perpendicular to y such that the coordinate system is right handed (positive x is up in Fig 2a).

	$\langle N_x \rangle$	$\langle N_y \rangle$	$\langle N_z \rangle$	n_η	# N's
Front: 600 RPM	-0.15	-0.70	-0.69	1.36	1430
Front: 1200 RPM	0.02	-0.72	-0.68	1.20	1500
Front: 1800 RPM	-0.05	-0.76	-0.65	1.54	1536
Back: 600 RPM	-0.23	0.56	-0.79	1.32	1385
Back: 1200 RPM	0.07	0.70	-0.71	1.12	1405
Back: 1800 RPM	-0.11	0.70	-0.70	1.55	1550

Table 1

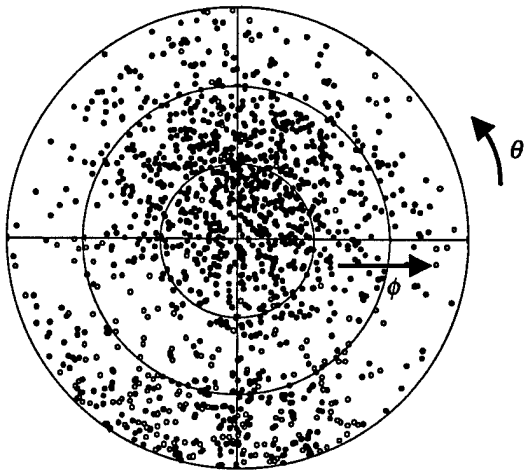

Figure 4. Hemisphere plot of surface normal vectors measured at 600 RPM. $\phi = 0$, 180° is located at the center of the "cross-hairs", with each concentric circle representing 30° increments of ϕ. Closed circles indicates normals in the range $\phi = 0$ to 90°. Open circles indicate normals in the range $\phi = 90$ to 180°.

Fig. 4 is a hemisphere plot showing N's measured on the front side of the kernel at the 600 RPM engine speed. The closed dots indicate normals in the range $\phi = 0$ to 90°, while open circles indicate normals in the range $\phi = 90$ to 180°. Crossed-plane tomography measurements are inherently crossing-weighted [2]: the probability of a certain N being measured is proportional to the probability that a flamelet surface with orientation given by N crosses the measurement line. We define a surface-weighted PDF, $P_s(\phi, \theta)$, such that $P_s(\phi, \theta)\, d\Omega$ is proportional to the fraction of the surface area with its normal within the solid angle $d\Omega = \sin\phi\, d\phi\, d\theta$. Following Corrsin [8], it can be shown that the surface-weighted PDF is related to the crossing-weighted PDF by $P_c(\phi, \theta) \propto P_s(\phi, \theta)\, |\mathbf{N} \bullet \mathbf{n}_\eta|$, where $\mathbf{n}_\eta$ is a unit vector in the direction of the measurement line.

Fig. 5 shows measured marginal, crossing-weighted PDF's of the polar angle, $P_c(\phi)$, for the front and back side of the kernel. It can be seen that there is little variation in $P_c(\phi)$ with engine speed. Measured marginal, crossing-weighted PDF's of θ, $P_c(\theta)$, had little variation as well. In previous work[6], it was shown that for turbulent V-flames there is no preferred azimuthal direction with respect to the mean normal, i.e. the surface-weighted marginal PDF of θ, $P_s(\theta)$, is constant. It was also shown that the surface-weighted joint PDF could be fit by $P_s(\phi, \theta) = A\, exp(-\phi^2/\zeta^2)$, where A is a normalization constant and ζ is a fit parameter. This fit was applied to the 600 RPM front side data, Fig. 6, for $\zeta = 65°$. The fit for $P_c(\phi)$ is in reasonable agreement with the data. It should be noted that the fit of $P_c(\theta)$ is not constant due to the contribution of the crossing-weighting factor, $|\mathbf{N} \bullet \mathbf{n}_\eta|$. The difference between the fit and the measured PDF's indicates that the N distribution is not symmetric in θ about <N>, but rather that a direction more downward than <N> in the vertical plane is a preferred orientation.

Conclusions

Crossed-plane imaging by acetone LIF was successfully applied to measuring N distributions in an optically accessible IC engine. The PLIF signal was sufficient to generate good contrast between product and reactant regions in the images. Interference from the edge-on laser sheet was completely eliminated through the use of an optical delay loop and gated, intensified CCD cameras. The optical access of the engine was sufficient for measurements to be made. Enough data were compiled to generate a reasonable statistical sample. A fit for the

surface weighted joint PDF $P_s(\phi,\theta)$ resulted in good agreement between the corresponding crossing-weighted marginal PDF in ϕ and the measured data. The difference between the crossing-weighted marginal PDF in θ and the measured data indicates that **N** distributions are not symmetrical in rotation with respect to <N>, unlike previous work on V-flames.

The burning rate in an engine is expected to increase with engine speed. From Eq. 1, it is therefore expected that there will be an associated increase in Σ with engine speed. Little variation in surface normal distributions were observed for the different engine speeds, and the trend in crossing density is not consistent with the expected increase in Σ, Eq. 2. Further analysis of the data is required to explore this inconsistency. Additional data were taken with an alternative camera and laser-sheet arrangement so that **N** distributions could be measured earlier in the flame kernel's evolution, and measurements were made at different stages in the kernel's evolution. Results of the analysis of images taken in this alternative arrangement as well as further analysis of the current data will be presented in a future paper.

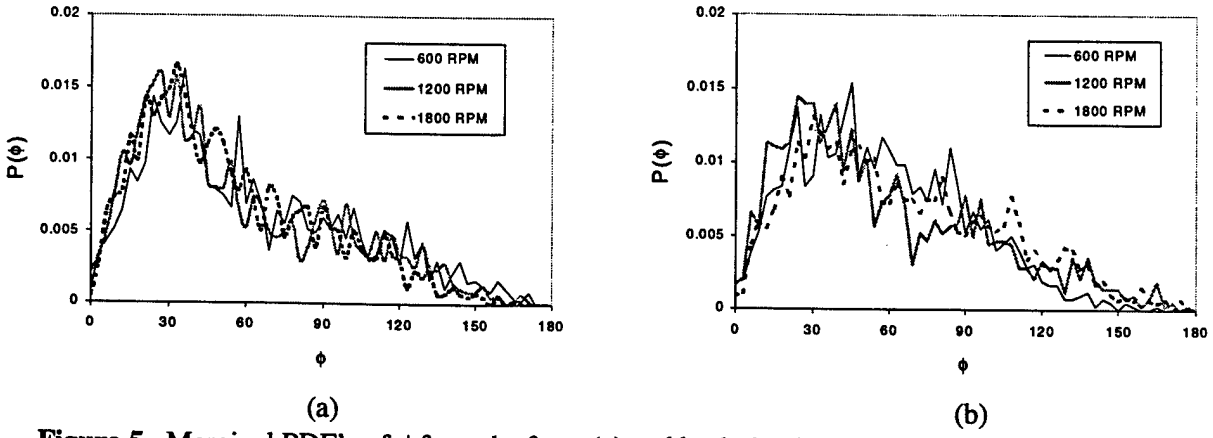

Figure 5. Marginal PDF's of ϕ from the front (a) and back (b) side of the kernel at the engine speeds studied.

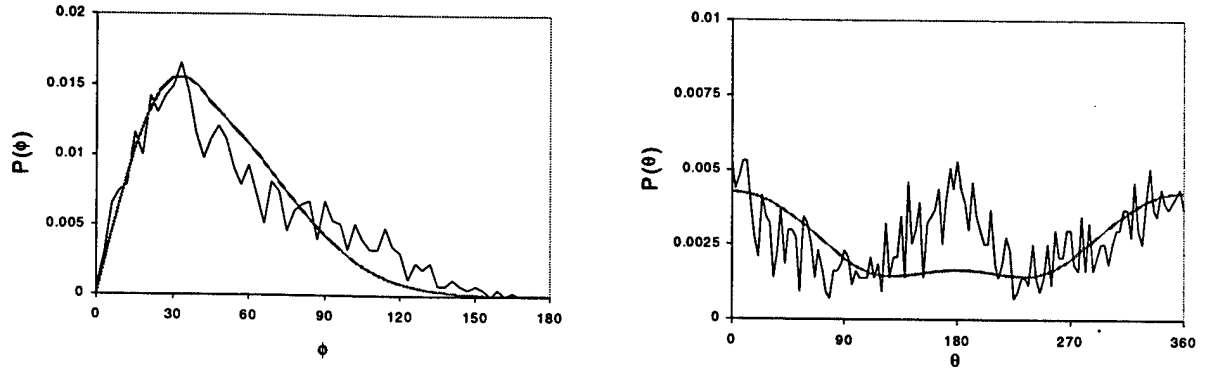

Figure 6. Crossing-weighted, marginal PDF's of ϕ and θ for the 600 RPM engine speed. The crossing-weighted, joint PDF is fit by $P_c(\phi,\theta)\ \sin\phi\, d\phi d\ \theta = A\ |\mathbf{N}\bullet\mathbf{n}_\eta|\ exp(-\phi^2/\zeta^2)\ \sin\phi\, d\phi\, d\theta$, $\zeta = 65°$.

References

1. Bray, K. N. C., Libby, P. A., Moss, J. B.: *Comb. Sci. Tech.* **41**, 143 (1984).
2. Gouldin, F. C. in *Physical and Chemical Aspects of Combustion: A Tribute to Irvin Glassman*, p. 433, Gordon and Breach, 1997.
3. Boyer, L. (1980): *Comb. Flame* **39**, 321.
4. Deschamps, B. M., Smallwood, G. J., Prieur, J., Snelling, D. R., Gülder, Ö. L. (1996). *Twenty-sixth Symposium (International) on Combustion*, The Combustion Institute, pp. 427-435.
5. Bingham, D. C., Gouldin, F. C., Knaus, D. A. (1998). Accepted for the *Twenty-seventh Symposium (International) on Combustion.*
6. Bingham, D. C. (1998). Crossed-Plane Laser Tomography: Direct Measurement of Flamelet Orientation and Mean Flamelet Surface Density. M.S. thesis, Cornell University.
7. Knaus, D. A., Gouldin, F. C., Bingham, D. C., in preparation.
8. Corrsin, S.: *Quart. Appl. Math. 12*, pp. 404-408, 1954.

Assessment of Crossed-Plane Tomography for Flamelet Surface Normal Measurements

D. A. Knaus, F. C. Gouldin and D. C. Bingham

A recently introduced method for measuring three-dimensional flamelet surface normal vectors, **N**, in turbulent, premixed flames in the flamelet regime is described and evaluated. Crossed-plane tomography allows the determination of **N** from two simultaneously acquired laser-tomographic images. The method is evaluated through comparison with single-plane measurements made on a vortex-street perturbed V-flame, and through an error analysis. The standard deviation of the angle between **N**'s measured using crossed-plane tomography and a vertical plane perpendicular to the flame stabilizing rod is 3.7°, consistent with the two-dimensional structure of this flame. PDF's of angles within this vertical plane measured using both techniques are almost entirely within statistical uncertainty of one another. The results of analysis of random error due to electronic noise and marker are consistent with experimental results and allows uncertainty to be estimated through analytic expressions. The nature of PDF's generated by crossed-plane tomography measurements is discussed with regards to evaluation of the mean inverse cosine of **N** and an arbitrarily oriented line through the flame brush, y. The preferred orientation of y is perpendicular to $\langle c \rangle$ contours because in the laminar and isotropic flame limits the mean inverse cosine term is well behaved: for y parallel to $\langle c \rangle$ contours, the laminar limit explodes. A PDF fit from previous work (Bingham et. al, 1998) is used to evaluate the mean inverse cosine term: the maximum value is slightly more than two, indicating that large burning rate flames must have correspondingly large values of the mean flamelet crossing density.

I. Introduction

Premixed turbulent flames occur in several different classes of practical combustion devices including spark-ignition engines; premixed, prevaporized gas-turbine combustors; and industrial furnaces. The local structure of the reaction zone in these combustors varies depending on the conditions of combustion, e.g. the turbulence level, type of reactants and the local equivalence ratio. Different combustion regimes have been identified: wrinkled flamelets, corrugated flamelets, distributed reaction zones and the well-stirred reactor (Bray and Peters, 1994). For the flamelet regime, which includes wrinkled and corrugated flamelets, chemical reactions and gradients in scalar quantities are assumed to be confined to thin sheets separating regions of reactants from regions of products that, due to turbulent velocity fluctuations, are wrinkled on multiple scales and are constantly in motion. In this limit the scalar structure of the turbulent reaction zone is determined by the topography of the flamelet sheets and the structure of the associated thin flamelet transition zone, e.g. the distributions of scalar quantities and gradients across the flamelet.

It is generally accepted (Bray and Peters, 1994) that in the flamelet regime the mean rate of product formation can be expressed as the product of the mean flamelet surface area to volume ratio, or surface density, $\sum$, and the mean rate of product formation per unit flamelet surface area expressed as the mean of the flamelet burning rate integral $\langle B_L \rangle$ (Gouldin and Miles, 1995), Eq. 1. In making this statement, one neglects the correlation between the product formation rate and the instantaneous flamelet surface area in a small differential volume. Furthermore, one assumes that both a flamelet surface area and a rate of product formation per unit area can be defined, the strong flamelet assumption (Bray and Peters, 1994).

$$\langle w \rangle = \langle B_L \rangle \Sigma \qquad \text{Eq. 1}$$

The flamelet regime is generally associated with low to moderate levels of turbulence. The condition that the Kolmogorov scale of the turbulent velocity field must be larger than the thermal thickness of the flamelet is often cited as necessary for flamelets to exist. This condition implies that while flamelets are perturbed by curvature and imposed flow strain, the scales of these perturbations should be large compared to the thermal thickness of the flamelet. A consequence of this restriction is that temperature and species contours within flamelets are likely to be locally parallel or nearly parallel. This condition may be overly conservative; for example, small scale turbulence can distort the flamelet preheat zone considerably without a

similar distortion of the much thinner high temperature reaction zone. As long as one can identify a flamelet surface and determine $\langle B_L \rangle$ it seems reasonable to conclude that the strong flamelet assumption is valid. In previous work, a method to determine B_L and to define a flamelet surface were proposed (Gouldin and Miles, 1995).

The determination of $\sum$ and related quantities has attracted considerable attention. Several model equations and closures have been proposed (e.g., Cant et al., 1990, Borghi, 1990, Darabiha et al., 1989). The results of DNS have been used to find $\sum$ (e.g., Poinsot, 1996, Shepherd et al., 1992) and support closure model development for the terms appearing in various $\sum$ model equations. In a series of papers, Bray, Moss, Libby and Champion make use of the ideas of flamelet crossings of a point in space over time (Bray et al., 1984a) and along a line in space parallel to mean progress variable ($\langle c \rangle$) constant surfaces (Bray et al., 1984b) to develop closure models for $\langle w \rangle$ that in turn were interpreted to obtain expressions for $\sum$ (Bray et al., 1989). Subsequent to this work, Gouldin (1997) proposed an expression giving $\sum$ in terms of flamelet crossings of a line. By considering a small right cylinder of differential base area, dA, height dy, and arbitrary orientation, Fig. 1, it was shown that

$$\sum = \left\langle \frac{1}{|\mathbf{N} \cdot \mathbf{n}_y|} \right\rangle_c n_y. \qquad \text{Eq. 2}$$

$\mathbf{N}$ is the flamelet surface normal, directed towards reactants at the point where the surface crosses the axis, y, of the cylinder; $\mathbf{n}_y$ is a unit vector defining the orientation of this axis; and n_y is the average number of flamelet crossings per unit length of the line y. In Eq. 2, the average, denoted by the subscript c, is over all flamelet crossing events. Therefore, realizations for which $\mathbf{N}$ is perpendicular to $\mathbf{n}_y$ are not counted in the average, since the flamelet does not cross y in these cases, and the associated potential singularity is removed from Eq. 2. We will return to the evaluation of the average in Eq. 2 below.

There has been theoretical work for the flamelet regime wherein the flamelet is modeled as an interface with a propagation speed relative to the reactant flow (e.g., Williams, 1985, Bray and Peters, 1994, Peters, 1992). An equation for the surface motion is developed and solved numerically or analyzed further to obtain a moment equation requiring closure modeling. This work has given considerable insight into flamelet behavior and turbulent flame conditions.

Compared to the various modeling efforts, experimental efforts to measure $\sum$ and related quantities have been far less numerous. Until now, there have been no direct measurements of $\sum$ or quantities such as the flamelet normal or radii of curvature that help describe flamelet topography. Several investigators have reported two-dimensional image measurements made either by laser tomography or laser induced fluorescence imaging which have been used to infer $\sum$, frequently through use of the surface normal term in Eq. 2. Point measurements have also been used for this purpose, but the results can suffer from considerable uncertainty (Miles and Gouldin, 1992, Gökalp et al., 1998).

Examples of laser imaging measurements are the work of Chew et al. (1990), Shepherd and Ashurst (1992), Lee et al. (1992), Deschamps et al. (1996), and Veynante et al. (1996). In all these measurements, planar images are obtained and the curve defined by the intersection of the laser illumination plane and flamelet surface is determined. From such images, data on the curvature, orientation and length of these intersection curves have been extracted and used to infer $\sum$ in various ways. Since only the intersection *curve*, and not flamelet *surface*, is observed, the resulting values of $\sum$ are subject to an undetermined systematic error. Shepherd and Ashurst (1992) have addressed this problem by using numerical simulation results to estimate the error. Unfortunately, as discussed below, they make a mistake in implementing Eq. 2, and consequently, their results are in error.

Eq. 2 provides a basis for the determination of $\sum$ from measurements of $\mathbf{N}$ and n_y, and in this paper we present and evaluate a method for measuring these quantities using a dual plane tomography method we call crossed-plane tomography. $\mathbf{N}\bullet\mathbf{n}_y$ is the cosine of the acute angle between $\mathbf{N}$ and $\mathbf{n}_y$, and $\langle 1/|\mathbf{N}\bullet\mathbf{n}_y|\rangle_c$ is frequently referred to as the direction cosine term. When first introduced by Bray, Moss and Libby, $\mathbf{n}_y$ was a direction tangent to $\langle c\rangle$ constant surfaces, $\langle c\rangle$ contours. However, Gouldin's derivation of Eq. 2 (Gouldin, 1997) shows that $\mathbf{n}_y$ can be in any direction. Furthermore, Gouldin and Miles (1995) present arguments for why $\mathbf{n}_y$ perpendicular to $\langle c\rangle$ contours is the preferred direction, since with this choice $n_y = N_c \langle c\rangle (1 - \langle c\rangle)/l$ to first approximation and in the laminar limit $\langle 1/|\mathbf{N}\bullet\mathbf{n}_y|\rangle_c$ is bounded and the expression for $\sum$ approaches the correct limiting value smoothly.

There are several misinterpretations of Eq. 2 common in the literature. Adopting the notation $\sigma_y = \mathbf{N}\bullet\mathbf{n}_y$, Eq. 2 becomes

$$\Sigma = \left\langle \frac{1}{|\sigma_y|} \right\rangle_c n_y. \qquad \text{Eq. 2a}$$

Frequently, one finds this expression replaced by $(1 / \langle|\sigma_y|\rangle)\, n_y$, where the mean of the reciprocal is replaced by the reciprocal of the mean. Another misinterpretation is that the angle defining σ_y is taken to be the angle between **N** and its projection on a $\langle c \rangle$ constant surface and not the angle between **N** and a fixed line along which n_y is defined. This latter problem is found in Chew et al. (1990), and in Shepherd and Ashurst (1992) and may explain the difference between their results for $\langle 1/|\sigma_y| \rangle_c$ and those reported here and by Bingham et al. (1998). Furthermore, there is confusion regarding the averaging in Eq. 2, which, as discussed below, is over flamelet crossing events.

As noted, in this paper we report on a new method, crossed-plane laser tomography, which allows, for the first time, direct measurements of **N**, as well as measurements of n_y, to be made. The new method will be described, and the results of validation measurements on a laminar V-flame perturbed by a von Kármán vortex street will be reported. The evaluation of Σ from **N** data via Eq. 2 will be discussed; it will be shown that the average in Eq. 2 is over crossing events; and hence the singularity for $\mathbf{N} \bullet \mathbf{n}_y = 0$ is removed. Finally, some implications of the data for **N** in turbulent V-flames reported by Bingham et al. (1998) will be discussed.

II. Crossed-Plane Tomography

Concept:

Laser tomography, first described by Boyer (1980), allows for the visualization of the instantaneous location of a flamelet surface in a planar cross section of a turbulent premixed flame. Reactants are seeded with an aerosol of oil droplets, which evaporate upon reaching the flamelet surface. The flame is illuminated with a laser beam shaped into a thin sheet. The droplets in the reactants scatter the laser light; however in the products the droplets have evaporated, and no scattering occurs. The light scattered from the reactants is recorded as an image by a camera aligned normal to the laser sheet. For the image to be considered to be an instantaneous visualization of the flamelet surface location, the exposure time must be short compared to the characteristic time of the flamelet motion. Therefore, either the exposure time

of the camera, or the pulse duration of the laser, must be short. Because the image represents a two-dimensional cross section of the three-dimensional flamelet *surface*, the flamelet surface appears as a *boundary* in the image. The *flamelet boundary* is identified as the boundary between the illuminated reactant regions and the dark product regions in the image, and physically represents the instantaneous location of the flamelet in the cross sectional slice of the flame illuminated by the laser sheet.

Actual flamelet surfaces are typically three-dimensional structures. Single-plane laser tomography only provides information about the flamelet surface topography in the plane of the laser sheet, nothing is known out of this plane. Crossed-plane laser tomography allows measurement of the three-dimensional flamelet surface orientation, in the form of the flamelet surface normal vector, **N**, from two simultaneously acquired orthogonal images. Two orthogonal laser sheets intersect along a line within the flame, and simultaneous images from both sheets are recorded. Unit vectors tangent to the flamelet boundary are determined in the two images at the point where the boundaries traced in each image intersect, i.e. along the *line of intersection* of the two laser illumination planes. These two vectors are tangent to the flamelet boundary, and hence the flamelet surface, **N**, is the normalized cross product of these two vectors. Therefore, the orientation of the flamelet surface is defined in three-dimensions from the two-dimensional information obtained in each of the two images. Repeated measurements must be made to build a set of **N** data, as well as a set of data that can be used to determine n_y. Fig. 2 shows light scattered by the droplet seeded reactants above a V-flame burner as well as the Cartesian coordinate system used throughout this paper: the horizontal y-axis lies along the line of intersection of the laser illumination sheets in the direction of beam propagation, the x-axis is vertical, and the z-axis is horizontal, parallel to the flame stabilizer rod.

Implementation of crossed-plane tomography is complicated by the fact that at the location in one image where the tangent vector is to be determined, the flamelet boundary is obscured by light scattered from the other illumination sheet, which appears edge-on. To eliminate this interference, the polarizations of the light in the two sheets are aligned orthogonal to one another. Polarizing filters on the imaging cameras are then used to block light scattered from the edge-on beam, thereby allowing an unobscured view along the line of interest.

Apparatus:

Fig. 3 is a schematic of the experimental apparatus. Experiments are performed on a rod-stabilized V-flame burner described in Miles (1991) and Miles and Gouldin (1998). Commercial grade methane and air flow rates are controlled by mass flow meters. The flame conditions and measurement locations studied are summarized in Table 1. Air and fuel flows are premixed in a plenum at the base of the burner. Reactants are seeded via a blast atomizer-type seed particle generator, discussed below. A coaxial air flow is used to prevent interaction of the premixed jet with the quiescent laboratory surroundings in the region of the stabilized V-flame. The burner exit diameter is 50 mm. The V-flame is stabilized on a 1.65 mm rod positioned approximately 5 mm above the burner exit. The burner is mounted on traverses so that it may be moved in three orthogonal directions. The measurement height, defined as the vertical distance between the stabilizing rod and the line of intersection of the laser illumination sheets, is set by first raising the burner so that the line of intersection of the laser illumination sheets is incident on the stabilizing rod, and then lowering the burner to the desired height.

A 1 mm diameter rod is positioned parallel to the stabilizing rod, 2.5 mm upstream and 3.0 mm cross-stream from it and generates a von Kármán vortex street which perturbs one side of the V-flame. A vortex street perturbed flame is used to evaluate crossed-plane tomography because the two-dimensional structure of the vortex street induced flame perturbations allow direct comparison between crossed-plane tomography normal data and flamelet surface normals measured using single-plane tomography. A vortex street shed by a cylinder remains laminar and stable for Reynolds numbers less than 150 (Namer et al., 1984), maintaining its two-dimensional structure as it convects downstream. In the current work, the Reynolds number based on the vortex shedding rod diameter is 98. There have been numerous studies detailing the structure of vortex street perturbed V-flames, including Lee et al.(1993), Hetrzberg et al.(1984), and Namer et al. (1984). In the current work, the details of the flame are not important, except that the two-dimensional character is exploited in order to compare flamelet surface normal data obtained by both crossed-plane and single-plane tomography.

The seed particle generator seeds the reactants with a silicone-based oil chosen for its relatively low vaporization temperature, approximately 650 K (Miles, 1991). The mean droplet diameter generated by the atomizer is expected to be 1μm (Durst et al., 1981), with a small number of larger droplets, up to 100 μm, expected as well (Orr, 1966). These larger droplets are removed from the flow via a cyclone separator, which has a design collection efficiency greater

than 90% for 5 μm droplets, and the efficiency of the separator increases with particle size. To ensure proper location of the reactant-product boundary, it is critical that a negligible number of droplets penetrate the flame. Miles (1991) calculates that for this oil, all particles of diameter less than 5 μm will have evaporated before a local gas temperature of 800 K is reached. He further estimates that the flamelet boundary identified in the images represents the 650 K isotherm within the flamelet. In order that the seeding particles do not alter the structure of the flame, the sum of the energy consumed by evaporation and the energy released by the combustion of the oil particles must be small compared to the energy released by the combustion reactions themselves. Based on the estimates of Miles (1991), the maximum expected oil mass fraction is $4x10^{-4}$ grams of oil per gram of combustible mixture, which corresponds to a number density of approximately 1000 mm^{-3} for 1.0 μm diameter droplets (Miles 1991). Chew et al. (1989) found the effect of the oil droplets to be negligible for oil concentrations significantly greater than used in the current work.

Laser illumination sheets are generated by a frequency-doubled Nd:YAG pulsed laser (532 nm, 7 ns pulse duration), firing continuously at a 10 Hz rate. The laser is an unstable resonator so that the beam is not in a Gaussian mode, but in a higher order annular mode. The laser beam exits the frequency doubler vertically polarized with a 6.4 mm specified diameter (FWHM). The laser beam is split, and the polarization of each beam is rotated via a half wave plate such that the polarization is in the plane of the sheet that is generated from the beam. The beams are focused by 500 mm spherical lenses before passing through orthogonally aligned cylindrical lenses to form the laser illumination sheets. The maximum sheet thickness across the camera field of view is estimated to be less than 0.5 mm based ray tracing approximations. This estimate is confirmed visually by blocking the sheets at the edge of the field of view of the cameras with a black plate and measuring the sheet thickness on the plate with the laser firing at low intensity. The sheet thickness is expected to decrease at the higher laser intensities used in the actual experiment, due to the properties of the laser's optical cavity. Because of the annular mode of the laser beam, the laser sheet structure is actually that of two closely spaced, parallel sheets. The laser beam structure is therefore non-ideal for the experiment, but because the parallel sheets are close together across the field of view of the cameras, we can assume the structure is equivalent to one thin sheet with a nominal thickness of 0.5 mm. The sheets are at

45° angles, with an uncertainty of ±2°, to the horizontal in the laboratory reference frame so that the cameras may be positioned outside of the product/reactant flows.

Images are acquired by simultaneous exposure of two digital cameras that are triggered by a control pulse synchronized with the laser pulse. The cameras are positioned at 45° angles with respect to the horizontal, looking downward in the laboratory reference frame such that the optical axis of each camera is normal to one sheet and edge-on (parallel) to the other. The cameras record 256 gray-scale colors and contain 652x494 pixel CCD arrays. They are fitted with 50 mm focal length lenses and 10 mm extension tubes, providing a field of view of approximately 35 mm x 25 mm; polarizing filters to block light scattered from the edge-on beams; and 10 nm bandwidth laser line filters that block almost all flame radiation while passing the scattered laser light. Because the laser pulse duration is short compared to typical camera exposure times, the camera exposure is set to its minimum, 10 ms.

Single-plane measurements are made using the same experimental apparatus described above with some necessary modifications. One beam is blocked, while the other beam is formed into a vertically oriented sheet perpendicular to the flame stabilizing rod. Only one camera is necessary, and is positioned horizontally so that it is normal to the illumination sheet.

Analysis:

Because of the large size of the image files, image processing is performed in real time, and only flamelet surface normal vectors are stored. Image processing involves a series of steps, which are outlined here and then discussed in detail below. The first step is thresholding, in which the images are made binary by setting image pixels above a designated threshold to white, and image pixels below the threshold to black. Next, small-scale features (less than 4 pixels in diameter) are removed from the images through erosion and dilation of image pixels. The flamelet boundary is then identified by an edge-finding algorithm. So that a curve fit can be applied to the flamelet boundary, the boundary representation is transformed into parametric space. The parameterized boundary curve is then smoothed by simple averaging, and polynomial fits are applied in parametric space. **N** determinations are made where the flamelet surface crosses the line of intersection of the two laser illumination sheets. In each image, this line of intersection appears as the edge-on sheet, and its location in each camera's field of view is determined before taking actual measurements. The slopes of the polynomial fits at the line of intersection are then used to calculate the slope of the flamelet boundary. This is done for both

images, and the resulting slopes are used to define tangent vectors to the flamelet boundary in each image, which are then used to determine **N**.

The thresholding level is determined before data acquisition. In order that a clear distinction be made between product and reactant regions in the images, it is desirable to create as much contrast between the light (reactant) and dark (product) regions in the images as possible. This can be accomplished by setting the laser to a high intensity, such that most pixels in the reactant regions are saturated at the maximum gray scale level of 256, with most pixel levels in the product regions still at gray scale levels near 1. However, because not all light scattered from the edge-on beam is removed by the polarizing filter, the laser power level must be low enough so that interference from the edge-on beam in the product region of an image is below the threshold level. It is possible to set the laser intensity so that pixels in the reactant region are mostly saturated while interference levels from the edge-on beam are negligible. This laser intensity is determined before acquiring images for **N** calculations by observing images and setting the laser power appropriately. An intermediate threshold can then be chosen, typically around 100. Blooming (the bleeding of saturated pixel signals into neighboring pixels) is prevented by an anti-blooming feature of the cameras, so that the cameras can be operated at saturation levels without introducing error in measuring the location of the product/reactant interface (Walker, 1998).

The discrete nature of the oil droplets can result in the images containing black "islands", or small-scale black features in otherwise white regions of the thresholded images. A large droplet may briefly penetrate into the products, resulting in a white "island" in the products. It is necessary to eliminate these and other small scale irregularities in the images to decrease uncertainty in locating the flamelet boundary. To eliminate these islands as well as noise caused by occasional scan error of the CCD array, a process of opening followed by closing is used (Castleman, 1996). Opening a binary image involves a process of erosion followed by dilation. Erosion converts all image pixels within the dilation diameter of a white image pixel to white image pixels ("eroding" black pixels). Dilation converts all image pixels within the erosion diameter of a black image pixel to black image pixels ("dilating" black objects). Opening a binary image has the effect of eliminating all black features smaller than the erosion/dilation diameter, which was set at 4 pixels, or approximately 0.2 mm. This scale was selected by observation of recorded images, as a compromise between eliminating small scale "islands" in

the reactants and changing the actual flame structure. Closing an image is the opposite of opening: dilation followed by erosion. Closing has the effect of eliminating all white features smaller than the erosion/dilation diameter. The net effect is the removal of all features smaller than the erosion/dilation diameter, and the smoothing of white/black interfaces. The erosion/dilation diameter is selected to be small enough to preserve small scale physical features in the flame, while eliminating the small "islands" that make flamelet boundary identification difficult.

After this initial treatment of the images, the flamelet boundary is located by an edge-finding algorithm. The flamelet boundary is located in pixel coordinates, denoted χ and ξ with the χ axis parallel to a row of pixels and the ξ axis parallel to a column of pixels in an image. The edge-finding algorithm works by locating the point where the boundary intersects the top of the image, and then moving along the boundary down to the bottom of the image. The field of view of the cameras used to acquire the images is sufficiently wide that no intersections of the boundary occur with the right or left sides of the image. As a demonstration of how the algorithm works, consider an image which is black on the left and white on the right, with an irregular interface somewhere in the middle. The algorithm begins by "moving" along the top row of image pixels until it encounters a white image pixel. It then turns down and looks for a white image pixel. If there is a white image pixel down, the algorithm moves down, otherwise it continues along the top of the image. Every time the algorithm moves to a new image pixel, it first looks to the right from the direction it just moved for a white image pixel. If there is not a white image pixel, it rotates back to the left (counter-clockwise) looking for a white image pixel until it locates one, and then moves to the white image pixel. In this way the algorithm traces along the outermost edge of white image pixels along the interface. The image pixel location of each successive point along the boundary is stored in an array.

Next the boundary is smoothed and a curve fit is applied at the line of intersection. Because the boundary may not be single valued in pixel space, it is converted into a parameterized form and fit in parametric space. The array of boundary image pixels is parameterized in terms of the variable s, where s is a curvilinear coordinate along the boundary, yielding χ as a function of s and ξ as a function of s. The parameterized curves are smoothed by two iterations of simple smoothing (Castleman, 1996): each χ and ξ value is replaced by the average of the adjacent χ and ξ values over a smoothing width Δs. The first smoothing iteration

is over an 11 point smoothing width to smooth small scale roughness first, and the second iteration is over a 31 point width, smoothing on a larger scale. The smoothing widths and number of iterations were chosen by observing the effect of smoothing on the flamelet boundary in pixel space. After smoothing, second order polynomial, least-squares fits are made about the s location of the line of intersection of the laser sheets, where the tangent vectors are to be calculated. A higher order polynomial fit was not chosen because of increased computational time, and the second order polynomial fit matched the parameterized curves well. Determination of the location of the line of intersection is discussed later in this section. The width that the polynomial fit is applied over, which was determined by observing the resulting representations of the flamelet boundary on unprocessed images, is 51 points. The derivatives of the two fits, χ' and ξ', are evaluated, and the slope, m, of the boundary in pixel coordinates is calculated by

$$m = \frac{d\xi}{d\chi} = \frac{\xi'}{\chi'}.$$

Vectors tangent to the boundary at the line of intersection are calculated from this slope in each image, and the cross product of the two vectors is calculated and normalized to determine **N**, which is stored in an output file. Once image processing is complete, another pair of images is acquired, and the process repeats. The data rate is approximately one **N** measured every two seconds.

For single-plane tomography measurements, the same image processing is used, however the slope of the flamelet boundary is measured only in the one image, at the same flame location (height above the burner) as where the crossed-plane measurements were made. **N** is determined from this slope as a unit vector normal to the flamelet boundary, and is assumed to lie in the plane of the laser illumination sheet, the vertical plane, oriented into the reactants.

The image processing software may fail under certain circumstances, resulting in the program not processing an image pair further and no **N** value from the image pair being obtained. One event that can cause the software to fail is a situation in which a different number of flamelet crossings of the line of intersection are measured in the two images. Uncertainty in the location of the line of intersection in the two images may result in a flamelet cusp barely crossing the line of intersection in one image but missing the line of intersection in the other, causing a different number of flamelet crossings in the two images. Another problem that can

occur is that the edge-finding algorithm may become "trapped" in a closed region of the image and therefore never reaching the bottom of the image.

The determination of the location of the line of intersection in the laser illumination planes in each camera's field of view is extremely important: uncertainty in the location of this line in each image increases the possibility that the tangent vectors will not be measured at the same point on the flamelet surface. The procedure for identifying the line of intersection is carried out separately for each camera before data acquisition. The beam corresponding to the normal sheet is blocked, leaving only the edge-on beam. To observe the edge-on beam, the polarizing filter is turned slightly. An image is acquired, and the pixel of maximum intensity is found in each of the 652 vertical pixel columns of the image. To improve the probability of the pixel of maximum intensity in each column being found unambiguously, the laser intensity is set at a low level, so that no pixels in the image are near saturation. A linear fit is applied to these brightest pixels, and used to define the location of the edge-on beam, and hence the line of intersection. For single-plane measurements, the line of intersection is defined as a line of slope zero in pixel coordinates. The ξ location of this line is determined by raising the burner so that the stabilizing rod is near the middle of the field of view of the single camera, recording the ξ location of the stabilizing rod as the location of the line of intersection, and then lowering the burner to the desired measurement height.

III. Evaluation of Method: Measurements on a Perturbed Laminar V-Flame

To determine the accuracy of the crossed-plane laser tomography technique, crossed-plane and single-plane measurements made on a rod stabilized V-flame perturbed by a von Kármán vortex street are compared. The flame condition studied is outlined in Table 1. For crossed-plane measurements, 2000 image pairs were acquired, however 25 (1.25%) of the image pairs could not be processed. Normal vector orientations are described by two angles, ϕ and θ, with ϕ being the polar and θ the azimuthal angle with respect to the laser line of intersection, the y-axis. θ is defined such that the z-axis is at $\theta = 0°$. Ideally, all **N**'s would lie within a vertical plane reflecting the two-dimensionality of the perturbed flame; $\theta = 90°$ or 270°. Fig. 4 is a polar plot of the 1975 **N**'s measured by crossed-plane tomography. A majority of the data lie in a narrow vertical band close to this vertical plane. Some data lie noticeably out of this band, especially at ϕ's approaching 90°.

To quantify the two-dimensionality of the crossed-plane data and to make the comparison between single and crossed-plane measurements it is convenient to describe normal vector orientations in terms of two different angles, α and β. The angle α is defined as the angle between the normal, **N**, and its projection onto the vertical plane, $\mathbf{N}_{xy}$. The angle β is defined as the angle between $\mathbf{N}_{xy}$ and the y-axis. These angles are shown in Fig. 5. Data from single-plane tomography are assumed to lie in the vertical plane; $\alpha = 0°$ and β is the angle between **N** and the y-axis. If the data were perfectly two dimensional, a PDF of α measured using crossed-plane tomography would be a delta function at 0°. Ideally, PDF's of β generated using crossed-plane tomography and single-plane tomography would be identical.

Fig. 6 is a PDF of α measured using crossed-plane tomography. The PDF consists of a narrow spike at zero degrees. The departure of the measured normals from the expected behavior, that they would lie in a vertical plane perpendicular to the stabilizing rod, is quantified by the standard deviation of the PDF, which is 3.7°. Some of the width of the PDF may be attributed to three-dimensionality of the actual perturbed flamelet surface. Errors in the technique could also lead to the broadening of the α PDF. In Fig. 7, PDF's of β measured using crossed-plane and single-plane tomography provide a direct comparison between the two techniques. The majority of the difference between the two data sets is within the statistical uncertainty resulting from the finite number of measurements made. For the middle range of angles, the statistical uncertainty for each PDF is estimated to be ±13% (Tennekes et al., 1972), which is greater than the difference between the two data sets. However, at $\beta = 45°$ the PDF measured using crossed-plane tomography has a large spike that is not present in the single-plane PDF. The statistical uncertainty of each PDF is approximately ±10% at 45°, indicating an error in the crossed-plane measurements not associated with statistical uncertainty.

To discuss error in the measurement technique, we will refer back to the more general description of the surface normals, in terms of ϕ and θ. Random error in the calculation of **N** is caused by electronic noise and the discrete nature of the oil droplets. This random error introduces uncertainty in the slope of the flamelet boundary along the line of intersection in the two images. Random error is minimized through the smoothing and curve fitting routines. This error can be estimated based on the uncertainties in the polynomial least squares fit parameters, which are a reflection of the agreement of the fits with the parameterized flamelet boundary data.

Recall that for one image, the measured slope, m, is related to the derivatives of the parameterized curves by $m = \xi'/\chi'$, where ξ' and χ' denote derivatives of ξ and χ with respect to the curvilinear coordinate s. The least squares fits are of the form $\chi(s) = a_\chi + b_\chi s + c_\chi s^2$ and $\xi(s) = a_\xi + b_\xi s + c_\xi s^2$. The curvilinear coordinate s is shifted so that $s = 0$ at the location along the parameterized boundaries where χ' and ξ' are to be evaluated. This way the derivatives are easily calculated, $\chi' = b_\chi$ and $\xi' = b_\xi$. The expression for the fractional uncertainty in the measured slope, δm, is then

$$\frac{\delta m^2}{m^2} = \frac{\sigma_{b_\chi}^2}{b_\chi^2} + \frac{\sigma_{b_\xi}^2}{b_\xi^2} - 2\frac{\sigma_{b_\chi b_\xi}^2}{b_\chi b_\xi}, \qquad \text{Eq. 3}$$

where $\sigma_{b_\chi}^2$ and $\sigma_{b_\xi}^2$ are the variances of b_χ and b_ξ respectively and $\sigma_{b_\chi b_\xi}^2$ is the covariance of b_χ and b_ξ (Bevington and Robinson, 1992). Estimates for $\sigma_{b_\chi}^2$ and $\sigma_{b_\xi}^2$ are calculated by the fitting routine in the form of elements of the covariance matrix of each fit (Press et al., 1988). These terms are of the form $\sigma_{b_\chi}^2 = \sigma_\chi^2 f(s_i)$ and $\sigma_{b_\xi}^2 = \sigma_\xi^2 f(s_i)$, where σ_χ^2 and σ_ξ^2 are the uncertainties in the dependent variables, χ and ξ, and s_i are the values of the independent variable , s, used in the fits, $s_I = -25 \rightarrow 25$. The values of s_i are the same for both fits, and in turn $f(s_i)$ is the same for both fits. $\sigma_{b_\chi b_\xi}^2$ is of the form $\sigma_{b_\chi b_\xi}^2 = \sigma_{\chi\xi}^2 f(s_i)$, and $\sigma_{\chi\xi}^2$ is taken as the average of σ_χ^2 and σ_ξ^2, so that the final expression for the covariance term is $\sigma_{b_\chi b_\xi}^2 = (\sigma_{b_\chi}^2 + \sigma_{b_\xi}^2)/2$ (Bevington and Robinson, 1992). Analysis of the random error in θ, $\delta\theta$, and in ϕ, $\delta\phi$, due to the uncertainty in the measured slopes, m_a and m_b, yields the expressions

$$\delta\theta^2 = \frac{(m_b \delta m_a)^2 + (m_a \delta m_b)^2}{(m_a^2 + m_b^2)^2} \quad \text{and} \quad \delta\phi^2 = \frac{(m_b^3 \delta m_a)^2 + (m_a^3 \delta m_b)^2}{(m_a^2 + m_b^2)(m_a^2 m_b^2 + m_a^2 + m_b^2)^2},$$

where δm_a and δm_b are the uncertainties in m_a and m_b, obtained from Eq. 3. ϕ and θ are related to m_a and m_b by

$$\phi = \text{acos}\left[\left(1+\frac{1}{m_a^2}+\frac{1}{m_b^2}\right)^{-1/2}\right] \quad \text{and} \quad \theta = \text{atan}\left(\frac{m_a}{m_b}\right). \quad \text{Eqs. 4a and b}$$

For the perturbed laminar V-flame, $m_a \cong m_b = m$. Assuming the uncertainty in the measurement of the slopes is equal, δm, the expressions for $\delta\theta$ and $\delta\phi$ reduce to

$$\delta\theta = \frac{\sqrt{2}}{2}\frac{\delta m}{m} \qquad \text{and} \qquad \delta\phi = \frac{\delta m}{m^2+2}. \qquad \text{Eqs. 5a and b}$$

A test image was analyzed, and m, δm, $\delta\theta$, and $\delta\phi$ were determined at different locations along the flamelet boundary. It was assumed that $m_a \cong m_b = m$, so that only one image was analyzed, and Eqs. 5a and b were used to evaluate $\delta\theta$ and $\delta\phi$. The uncertainties $\delta\theta$ and $\delta\phi$ are plotted in Fig. 8 as a function ϕ. $\delta\phi$ is small, with an average value of 0.5°, and appears constant over ϕ. The average uncertainty in θ is 2.6°, and becomes large as $\phi \rightarrow 0°$. As ϕ goes to its limits, 0° and 90°, m goes to ∞ or 0, respectively (Eq. 4a). For these limits, either b_χ or b_ξ goes to zero, $m = b_\xi / b_\chi$, resulting in a singularity in $\delta m/m$ (Eq. 3). It is therefore believed that $\delta\theta$ will become large as $\phi \rightarrow 90°$, although as seen in Fig. 8, no large ϕ's were measured in the test image. The increase in $\delta\theta$ as ϕ becomes large is apparent in Fig. 4 in the broadening of the vertical band as $\phi \rightarrow 90°$. The increase in $\delta\theta$ as $\phi \rightarrow 0°$ is not seen in Fig. 4 because as $\phi \rightarrow 0°$, **N** becomes parallel to the polar axis, and a large error in θ does not result in a large displacement of the normal on the unit sphere. For $\sum$ calculation, the contribution of normals as $\phi \rightarrow 90°$ is small because the crossing probability goes to zero, minimizing the effect of large $\delta\theta$ in this limit. The explosive limiting behavior observed in the $\delta\theta$ data in Fig. 8 is not seen in the $\delta\phi$ data. As $\phi \rightarrow 0°$, m becomes large. For large m, $\delta\phi$ is proportional to $1/m^2$, Eq. 5b, so that the denominator grows faster than the numerator. For $\phi \rightarrow 90°$, m goes to zero. For small m, the denominator of Eq. 5b is bounded by 2, and δm remains finite.

Systematic error is introduced into the measurements in several ways, including uncertainty in the location of the line of intersection; non-perpendicular laser sheets; arbitrary threshold selection; finite laser "sheet" thickness, so that an *area* of the flamelet surface is actually intersected; and the least squares fitting process itself. The experiment is designed to minimize systematic error as much as possible, through the routine that determines the line of intersection; proper alignment of the laser sheets; maximizing contrast between product and

reactant regions in the images so that the thresholding is as effective as possible; minimize laser-sheet thickness with optics; and selecting the curve fit parameters so that the fit matches the actual flamelet boundary as consistently as possible. The effect of some of these errors on **N** measurement are discussed below.

The angle of the laser sheets with the vertical plane was measured, and the sheets were within ±2° of 45° from vertical. A simulation program was written, in which surface normals are randomly generated in the *x-y* plane, like the perturbed laminar flame surface normals. The angle of the laser sheets with respect to vertical, which should be 45° for each sheet, were defined off 45°, simulating a systematic error in the angle of the sheets, and the result on the measured normals was studied. The result is a rotation of the measured normals about the polar axis. This sort of error would be apparent in Fig. 4, as the narrow band of measured normals would be rotated about the polar axis at some angle. It was found that for one sheet at 49° with the other properly aligned at 45°, the average error in ϕ is 0.25°, and the average error in θ is 2.0°. If one sheet is at 55°, the average error in ϕ is 1.5°, and the average error in θ is 5°. The fact that the surface normals measured in Fig. 4 appear to lie in a vertical band without rotation about the polar axis indicates that the sheets are well aligned and that there is little systematic error introduced into the measurements in this way.

It is obvious that tangent vectors must be measured on the line of intersection of the two planes in each image for the experimentally determined surface normal to correctly measure **N**. Uncertainty in the location of the line of intersection in each image results in tangents not being evaluated at the same location on the flamelet surface. This becomes even more important near cusps, where small errors in the determination of the location of the line of intersection may result in significant differences in measured slope due to the rapid change in slope with position along the flamelet boundary in the vicinity of the cusp. Determination of the location of the line of intersection is limited by the fact that the laser sheet has a finite thickness. Error analysis based on the linear least squares fit parameters indicates that the corresponding uncertainty in the vertical location of the line of intersection is ±0.2 mm, which is small compared to the nominal sheet thickness across the field of view of 0.5mm.

The small deviation from the *x-y* plane of the crossed-plane tomography data, seen in the α distribution in Fig. 6, as well as the good agreement found between β distributions measured using crossed-plane and single-plane tomography, Fig. 7, is an indication that systematic and

random errors in the new technique are small, and that crossed-plane tomography is a valid and accurate method, as well as the only method, for measuring flamelet surface normals.

IV. Evaluation of $\sum$ from N Data

N data measured using crossed-plane tomography can be used to evaluate $\sum$ via Eq. 2. As noted in the Introduction, the development in Gouldin (1997) leading to Eq. 2 averages over realizations in which the flamelet crosses a differential right cylinder (Fig. 1), i.e. the average is over crossing events. To properly evaluate $\sum$, it is therefore important to understand the nature of crossing-weighted averaging.

To discuss this averaging further, we introduce the surface-weighted PDF of **N**, $P_s(\theta,\phi)$. As above, **N** can be specified by two angles in spherical coordinates, $\mathbf{N}(\theta,\phi)$, and the PDF of **N** can be written in terms of these angles, $P(\theta,\phi)$. The surface-weighted PDF, $P_s(\theta,\phi)$, is defined such that $P_s(\theta,\phi)\ \sin\phi d\phi d\theta$ is proportional to the fraction of the surface area with θ and ϕ in the ranges θ to $\theta + d\theta$ and ϕ to $\phi + d\phi$, i.e., in the solid angle $d\Omega = \sin\phi\ d\phi\ d\theta$.

To transform the surface-weighted PDF to a crossing-weighted PDF, we represent the surface by covering it with a set of planar disks of differential area ds. The orientation of each disk is given by $\mathbf{N}(\theta,\phi)$, and the fraction of all disks having an orientation from θ and ϕ to $\theta + d\theta$ and $\phi + d\phi$ is just $P_s(\theta,\phi)\ d\Omega(\theta,\phi)$*. The probability that a disk is intersected by a line is proportional to the area of the disk projected normal to the line; i.e., proportional to $|\mathbf{N}\bullet\mathbf{n}_z|\ ds$, where $\mathbf{n}_z$ defines the orientation of the line in question. It follows that

$$P_c(\theta,\phi) = |\mathbf{N}\bullet\mathbf{n}_z|\ P_s(\theta,\phi) \Big/ \int_0^{2\pi}\int_0^{\pi} |\mathbf{N}\bullet\mathbf{n}_z|\ P_s(\theta,\phi)\ \sin\phi d\phi d\theta,$$

where the denominator insures normalization of the crossing-weighted PDF, $P_c(\theta,\phi)$. It is this PDF that is used to evaluate the direction cosine term in Eq. 2,

$$\left\langle \frac{1}{|\mathbf{N}\bullet\mathbf{n}_y|} \right\rangle_c = \int_0^{2\pi}\int_0^{\pi} P_s(\theta,\phi)\sin\phi d\phi d\theta \Big/ \int_0^{2\pi}\int_0^{\pi} |\mathbf{N}\bullet\mathbf{n}_y|\ P_s(\theta,\phi)\sin\phi d\phi d\theta,$$

or

*Note that for cases where $P_S = P_S(\theta,\phi,x,t)$, P_S is defined over an appropriate ensemble.

$$\left\langle \frac{1}{|\mathbf{N}\bullet\mathbf{n}_y|} \right\rangle_c = \frac{1}{\langle |\mathbf{N}\bullet\mathbf{n}_y| \rangle_s}.$$

s denotes a surface-weighted average; c a crossing-weighted average; and $\mathbf{n}_y$ defines the line crossed. Here it is worth noting that $P_c(\theta,\phi)$ is a function of the orientation of the line crossed.

The requirement for crossing-weighting was recognized by Corrsin (1954) who showed that for an isotropic distribution of $\mathbf{N}$, $P_s(\theta,\phi) = (4\pi)^{-1}$, and

$$\left\langle \frac{1}{|\mathbf{N}\bullet\mathbf{n}_y|} \right\rangle_c = 2 .$$

To investigate crossing-weighting further, we consider a simple two-dimensional analog of a wrinkled surface, a square wave of wavelength L and amplitude a (Fig. 9). For this case, the analog to $\sum$ is the mean length to area ratio, Λ, which for the square wave is simply $\Lambda = 2/L + 1/a$. The line normal orientation can be specified by its angle with respect to the vertical, ϕ, and its length weighted PDF is tri-modal: $P_l(\phi) = [a\,\delta(\phi+\pi/2) + L\delta(\phi) + a\delta(\phi-\pi/2)] / (2a+L)$. In the two-dimensional limit Eq. 2 is just

$$\Lambda = \left\langle \frac{1}{|\mathbf{N}\bullet\mathbf{n}_y|} \right\rangle_c n_y . \qquad \text{Eq. 2b}$$

For $\mathbf{n}_y$ in the vertical direction, the crossing density, n_y is $1/a$. Then

$$\left\langle \frac{1}{|\mathbf{N}\bullet\mathbf{n}_y|} \right\rangle_c = \frac{1}{\langle |\mathbf{N}\bullet\mathbf{n}_y| \rangle_l} = \frac{2a+L}{L}, \text{ and } \Lambda = \frac{2a+L}{L}\frac{1}{a} = 2/L + 1/a .$$

Alternately for $\mathbf{n}_y$ in the horizontal direction, the crossing density is $2/L$;

$$\left\langle \frac{1}{|\mathbf{N}\bullet\mathbf{n}_y|} \right\rangle_c = \frac{2a+L}{2a}, \text{ and } \Lambda = 2/L + 1/a$$

as before. In this example, both orientations considered for $\mathbf{n}_y$ have parallel line segments, $\mathbf{N}\bullet\mathbf{n}_y = 0$, that do not contribute to the crossing-weighted average in Eq. 2b and in both cases the correct value for Λ is obtained from this equation.

Having discussed the nature of the average in Eq. 2 and shown how that average can be evaluated beginning with the surface area weighted PDF for the normal **N**, we close by noting that different methods for finding **N** may have different weightings. Clearly, crossed-plane tomography yields **N** data that are crossing-weighted and can be used directly to construct $P_c(\theta,\phi)$. However, some uncertainty is likely to arise in these measurements from realizations where **N** is nearly perpendicular to the line of intersection of the two illumination planes, and the distinction between a crossing or no crossing is ambiguous. For another example, consider DNS results, clearly the PDF weighting will depend on the extraction process giving **N** from the computational results.

IV. Turbulent Flame Measurements

Crossed-plane tomography has been applied to measurements in turbulent V-flames (Bingham et al., 1998). Data for **N** were collected along a horizontal line spanning the turbulent flame brush, the *y*-axis, Fig. 2. For these data, the vortex-generating rod was removed, and replaced by a turbulence generating grid 50 mm upstream of the stabilizing rod. The grid is a square wire mesh type, with approximately 4.5 squares per cm^2 and a 1 mm wire diameter. Three turbulent flames were studied, with measurements of **N** made at two different axial (x) locations in each flame. For each of the flame conditions and measurement locations studied, data sets of approximately 1000 normals were obtained and then analyzed to find $P_c(\theta,\phi)$ and $P_s(\theta,\phi)$. The polar axis is aligned with the mean of the normal, <**N**>, and estimates for $P_c(\theta,\phi)\sin\phi d\phi d\theta$ were fit to the form $P_c(\theta,\phi)\ \sin\phi d\phi d\theta = C\ |\sigma_y|\ e^{-(\phi/\zeta)^2}\ \sin\phi d\phi d\theta$, where C is the normalization constant, σ_y is the cosine of the angle between **N** and the *y*-axis, and ζ is the fitting parameter. (NB: this fit implies that $P_s(\theta,\phi) = C\ e^{-(\phi/\zeta)^2}$.) Given the symmetry of V-flames, the uniform distribution with respect to rotation about the polar axis is not surprising. Typical PDF results from these measurements are shown in Fig.'s 10 and 11, and the flame conditions and ζ values for the measurements reported in Ref. 5 are shown in Table 1. The fluctuations seen in the azimuthal angle distributions are attributed to statistical noise due to the limited sample size. Furthermore, because of the small sample size no attempt has been made to find $P_c(\theta,\phi)$ as a function of position along *y*.

As noted above, Corrsin has shown that, for an isotropic distribution of **N**, $<1/|\mathbf{N}\bullet\mathbf{n}_y|>_c$ = 2 for any $\mathbf{n}_y$. For a laminar flame with $\mathbf{n}_y$ normal to the flame, normal to c contours, $<1/|\mathbf{N}\bullet\mathbf{n}_y|>_c$ = 1. Given these two limits it is interesting to speculate about the variation of $<1/|\mathbf{N}\bullet\mathbf{n}_y|>_c$ between them, for the case where $\mathbf{n}_y$ is locally normal to $<c>$ contours, as well as the case where $\mathbf{n}_y$ is perpendicular to $<c>$ contours. If the direction cosine term for $\mathbf{n}_y$ perpendicular varies monotonically between 1 and 2, then high values of $\sum$ are associated with large values of n_y, multiple flamelet crossings. If we assume that the form for $P_s(\theta,\phi)$ observed in the low turbulence level flames of Ref. 5 is valid for all turbulence levels, then we can use this form to find $<1/|\mathbf{N}\bullet\mathbf{n}_y|>_c$ as a function of ζ, the fitting parameter, which we expect to increase monotonically with turbulence level for a given flame configuration and fuel-oxidizer mixture. The result of this analysis for $\mathbf{n}_y$ perpendicular to $<c>$ surfaces is shown in Fig. 12, where it is seen that the direction cosine term varies nearly monotonically from 1 to 2. For comparison, the same analysis is performed for a distribution of the form

$$P_s(\theta,\phi) = \mathrm{C},\ \phi \le \zeta$$
$$= 0,\ \phi \ge \zeta .$$

In this latter case, also shown in Fig. 12, a small local maximum is observed in the curve of $<1/|\mathbf{N}\bullet\mathbf{n}_y|>_c$ vs. ζ. From the results of this exercise, we conclude that large values of $<1/|\mathbf{N}\bullet\mathbf{n}_y|>_c$, if they occur, come from distributions of ϕ that are skewed to values of ϕ near $\pi/2$, a situation that seems physically unlikely for a range of different flame geometry's.

It is important to note that the first two results presented in Fig. 12 are for $\mathbf{n}_y$ perpendicular to $<c>$ contours. Also shown in Fig. 12 is the result if $\mathbf{n}_y$ is taken to be parallel to $<c>$ contours and $P_s(\theta,\phi)$ is $\mathrm{C}\ e^{-(\phi/\zeta)^2}$ as before. For this case, the direction cosine term varies nearly monotonically from ∞ to 2, with 2 being the limiting values as $\zeta \rightarrow \infty$. This behavior is one reason why in our opinion $\mathbf{n}_y$ perpendicular to $<c>$ contours is the preferred choice over $\mathbf{n}_y$ parallel to $<c>$ contours.

Since values of the direction cosine term are likely to be limited in many turbulent flames, high values of the burning rate integral depend on n_y and its integral across the flame

brush, N_c. In turn high values of N_c occur from multiple flamelet crossings of y over the turbulent flame brush and depend on turbulence levels, and most likely, on the mean flame geometry and mean flow field. In view of the importance of N_c in determining the burning rate integral and the ease of measuring it via laser tomography, we suggest that investigators measure N_c for a wide range of conditions and flame geometry's (e.g. Bunsen flame, V-flame and stagnation flame) in order to determine its dependence on mean flame geometry and mean flow field, distinct from its dependence on turbulence level. The former dependence, if it exists, is clearly problem specific, while there may be general universality in the latter dependence.

VI. Summary

A new technique, crossed-plane laser tomography, has been developed, allowing direct measurement of the flamelet surface normal vector in turbulent premixed flames within the flamelet regime. The technique allows measurement of three-dimensional surface normals from two simultaneously acquired, orthogonal laser tomographic images. The method has been validated through measurements made on a perturbed laminar V-flame. The two-dimensional flame structure of the vortex street perturbed V-flame allowed a direct comparison to be made between crossed-plane and single-plane tomography measurements. The standard deviation of the angle between the surface normals measured using crossed-plane tomography and a vertical plane perpendicular to the stabilizing rod was 3.7°, consistent with the flame's two-dimensional structure. PDF's of the angle in this vertical plane measured both by crossed and single-plane tomography were almost entirely within statistical uncertainty of one another. Random error analysis demonstrated that uncertainty in the technique caused by electronic noise and the discrete nature of the oil droplets is small, except for $\phi \rightarrow 0°$ and $\phi \rightarrow 90°$, where the effect of the uncertainty has a limited effect on the calculation of the mean inverse cosine term in Eq. 2. Systematic error in the technique was discussed, with the accuracy of the validation measurements demonstrating that systematic error can successfully be limited in the technique.

It is important to distinguish between different types of averaging when determining PDF's from **N** data. The averaging in Eq. 2 is crossing-weighted, as are crossed-plane tomography measurements inherently. Other methods of gathering **N** data may be weighted in other ways, so that PDF's generated from other techniques must be converted to crossing-weighted PDF's before using Eq. 2, or the proper form of Eq. 2 (crossing-weighted, surface

weighted) must be used. The crossed-plane tomography technique was used to generate crossing-weighted and surface-weighted PDF's of **N** in several turbulent V-flames. The PDF's generated by these measurements are shown to be completely characterized by the fit parameter ζ. A fit of the crossing-weighted PDF of the form $P_c(\theta,\phi) = C\,|\sigma_y|\,e^{-(\phi/\zeta)^2}$ was used to evaluate the mean inverse cosine term in Eq. 2 as a function of ζ. In Eq. 2, $\mathbf{n}_y$ may be oriented in any direction. For $\mathbf{n}_y$ oriented perpendicular to $\langle c \rangle$ surfaces, the mean inverse cosine term is bounded by one in the laminar limit, and two in the isotropic limit. Because these limits are well behaved, as opposed to the mean inverse cosine term being unbounded in the laminar limit for $\mathbf{n}_y$ oriented parallel to $\langle c \rangle$ surfaces, this orientation is preferred. The fit for the crossing-weighted PDF's measured in turbulent V-flames was used to evaluate the mean inverse cosine term as a function of the fit parameter, ζ. The maximum value of the mean inverse cosine found in this way is slightly more than two, suggesting that in order to have a large burning rate for this type of flame, n_y must be large.

Future plans include measurements on higher turbulence level flames than those studied to date to test the PDF fit and allow empirical information to be gathered on the nature of the PDF and of n_y. Measurements are planned on different flame geometry's, particularly on a stagnation plate burner with axial symmetry. The effect of stable and unstable preferential diffusion conditions on **N** distributions will be studied. Measurements are also planned in the cylinder of a spark ignition engine with optical access. Improving data rates will allow larger data sets to be compiled, and variations in statistics with $\langle c \rangle$ across the flame brush will then be studied.

REFERENCES

Bevington, P. R., Robinson, D. K. (1992). *Data reduction and Error Analysis for the Physical Sciences*. McGraw-Hill, New York.

Bingham, D. C., Gouldin, F. C., Knaus, D. A. (1998). Crossed-Plane Laser Tomography: Direct Measurements of the Flamelet Surface Normal. Accepted for the *Twenty-seventh Symposium (International) on Combustion.*

Bingham, D. C. (1998). Crossed-Plane Laser Tomography: Direct Measurement of Flamelet Orientation and Mean Flamelet Surface Density. M.S. thesis, Cornell University.

Borghi, R. (1990). Turbulent Premixed Combustion: Further Discussions on the Scales of Fluctuations. *Comb. Flame* **80**, 304.

Boyer, L. (1980). A Laser Tomographic Study of a Laminar Flame in a Kármán Vortex Street. *Comb. Flame* **39**, 321.

Bray, K. N. C., Libby, P. A., Moss, J. B. (1984). Flamelet Crossing Frequencies and Mean Reaction Rates in Premixed Turbulent Combustion. *Comb. Sci. and Tech.* **41**, 143.

Bray, K. N. C., Libby, P. A., Moss, J. B. (1984). Scalar Length Scale Variations in Premixed Turbulent Flames. *Twentieth Symposium (International) on Combustion*, The Combustion Institute, pp. 421-427.

Bray, K. N. C., Champion, M., Libby, P. A. (1989). The Interaction Between Turbulence and Chemistry in Premixed Turbulent Flames. In *Turbulent Reactive Flows*, eds. R. Borghi and S. N. B. Murthy, Springer-Verlag, New York, p. 541.

Bray, K. N. C., and Peters, N. (1994). Laminar Flamelets in Turbulent Flames. In *Turbulent Reacting Flows*, eds. P. A. Libby and F. A. Williams, Academic Press, San Diego, Ch. 2, p. 63.

Cant, R. S., Pope, S. B., Bray, K. N. C. (1990). Modeling of Flamelet Surface-to-Volume Ratio in Turbulent Premixed Combustion. *Twenty-third Symposium (International) on Combustion*, The Combustion Institute, pp. 809-815.

Castleman, K. R. (1996). *Digital Image Processing*. 2nd Edition, Prentice Hall, Englewood Cliffs, New Jersey.

Chew, T. C., Britter, R. E., Bray, K. N. C. (1989). Laser Tomography of Turbulent Premixed Bunsen Flames. *Comb. Flame* **75**, 165.

Chew, T. C., Bray, K. N. C., Britter, R. E. (1990). Spatially Resolved Flamelet Statistics for Reaction Rate Modeling. *Comb. Flame* **80**, 65.

Corrsin, S., (1954). A Measure of the Area of a Homogeneous Random Surface in Space. *Quart. Appl. Math.* **12**, 404.

Darabiha, N., Giovangigli, V., Trouvé, A.Candel, S. M., Esposito, E. (1989). Coherent Flame Description of Turbulent Premixed Ducted Flames. In *Turbulent Reactive Flows*, eds. R. Borghi and S. N. B. Murthy, Springer-Verlag, New York, p. 591.

Deschamps, B. M., Smallwood, G. J., Prieur, J., Snelling, D. R., Gülder, Ö. L. (1996). Surface Density Measurements of Turbulent Premixed Flames in a Spark-Ignition Engine and a Bunsen-Type Burner using Planar Laser-Induced Fluorescence. *Twenty-sixth Symposium (International) on Combustion*, The Combustion Institute, pp. 427-435.

Durst, F., Melling, A., Whitelaw, J. H. (1981). *Principle and Practice of Laser Doppler Anemometry*. Academic Press, San Diego.

Ghenaï, C., Gouldin, F. C., Gökalp, I. (1998). Mass Flux Measurements for Burning Rate Determination of Premixed Turbulent Flames. Accepted for the *Twenty-seventh Symposium (International) on Combustion.*

Gouldin, F. C., Miles, P. C. (1995). Chemical Closure and Burning Rates in Premixed Turbulent Combustion. *Comb. Flame* **100**, 202.

Gouldin, F. C. (1997). Analysis of Certain Algebraic Closure Models for Premixed Turbulent Combustion. In *Physical and Chemical Aspects of Combustion: A Tribute to Irvin Glassman*, Gordon and Breach, Amsterdam, p. 433.

Hertzberg, J. R., Namazian, M., Talbot, L. (1984). A Laser Tomographic Study of a Laminar Flame in a Kármán Vortex street. *Comb. Sci. and Tech.* **38**, 205.

Lee, T. –W., North, G. L., Santavicca, D. A. (1992). Curveature and Orientation Statistics of Turbulent Premixed Flame Fronts. *Comb. Sci. and Tech.* **84**, 121.

Lee, T. –W., Lee, J. G., Nye, D. A., Santavicca, D. A. (1993). Local Response and surface Properties of Premixed Flames During Interactions with Kármán Vortex Streets. *Comb. Flame* **94**, 146.

Miles, P. C. (1991). Conditional Velocity Statistics and Time-Resolved Flamelet Statistics in Premixed Turbulent V-Shaped Flames. Ph.D. thesis, Cornell University.

Miles, P. C., Gouldin, F. C. (1992). Mean Reaction Rates and Flamelet Statistics for Reaction Rate Modeling in Premixed Turbulent Flames. *Twenty-fourth Symposium (International) on Combustion*, The Combustion Institute, pp. 477-484.

Miles, P. C., Gouldin, F. C. (1998). Premixed Turbulent Flame/Flow Interaction: Simultaneous Measurements of Velocity and Flamelet Position. *AIAA Journal* **36**, 1178.

Namer, I., Bill, R. G. Jr., Talbot, L., Robben, F. (1984). Density Fluctuations in a Flame in a Kármán Vortex Sheet. *AIAA Journal* **22**, 647.

Orr, C. (1966). *Particulate Technology*. MacMillan, New York.

Peters, N. (1992). A Spectral Closure for Premixed Turbulent Combustion in the Flamelet Regime. *Journal of Fluid Mechanics* **242**, 611.

Poinsot, T. (1996). Using Direct Numerical Simulations to Understand Premixed Turbulent Combustion. *Twenty-sixth Symposium (International) on Combustion*, The Combustion Institute, pp. 219-232.

Press, W. H., Flannery, B. P., Teukolsky, S. A., Vetterling, W. T. (1988). *Numerical Recipes in C: The Art of Scientific Computing*. Cambridge University Press, New York.

Shepherd, I. G., Ashurst, W. T. (1992). Flame Front Geometry in Premixed Turbulent Flames. *Twenty-fourth Symposium (International) on Combustion*, The Combustion Institute, pp. 485-491.

Tennekes, H., Lumley, J. L. (1972). *A First Course in Turbulence*. MIT Press, Cambridge, MA.

Veynante, D., Piana, J., Duclos, J. M., Martel, C. (1996). Experimental Analysis of Premixed Turbulent Combustion. *Twenty-sixth Symposium (International) on Combustion*, The Combustion Institute, pp.413-420.

Walker, J. N. (1998). Personal correspondence. Electrim Corp., Princeton, NJ, April 13.

Williams, F. A. (1985). Turbulent Combustion. In *Mathematics of Combustion*, ed. J. D. Buckmaster, SIAM, Philadelphia, Ch. 3, p. 97.

Flame	X (mm)	u (m/s)	u'/u_L	u_L (m/s)	Equivalence Ratio	Fit Parameter ζ (°)	$B_T/\rho_r\, u_L$
Perturbed Laminar	40	1.4	—	0.23	0.73	—	—
Turbulent 1	30	2.01	0.643	0.21	0.70	15.4	1.04
	80	2.47	0.685	0.21	0.70	25.5	1.15
Turbulent 2	80	4.30	0.956	0.21	0.70	37.7	1.30
	40	4.21	1.023	0.21	0.70	25.7	1.16
Turbulent 3	40	6.46	1.650	0.23	0.72	29.3	1.18
	80	6.42	1.732	0.23	0.72	39.5	1.32

Table I. Flame conditions and summary of turbulent V-flame results (Bingham et al., 1998).

Figure 1. Schematic representation of the intersection of a flamelet with a differential right cylindrical volume with orientation given by $\mathbf{n}_y$, a unit vector parallel to the cylinder axis.

Figure 2. Photograph showing laser-light scattered by aerosol of oil droplets seeded into reactants during crossed-plane tomography measurements on a perturbed laminar V-flame. Also shown is the Cartesian coordinate system used throughout the paper. The y-axis is coincident with the line of intersection of the two laser sheets.

Figure 3. Schematic of crossed-plane laser tomography apparatus.

Figure 4. Polar plot of 1975 **N**'s measured via crossed-plane tomography in the perturbed laminar V-flame. The polar axis is the line of intersection of the laser illumination sheets, the y-axis.

Figure 5. Angles used in the analysis of perturbed laminar flames. $\mathbf{N}_{xy}$ is the projection of **N** onto the x-y plane. α is the angle between **N** and $\mathbf{N}_{xy}$; β is the angle between $\mathbf{N}_{xy}$ and y.

Figure 6. PDF of α measured using crossed-plane tomography.

Figure 7. Comparison of PDF's of β measured using crossed-plane and single-plane tomography.

Figure 8. Uncertainty in the measurement of ϕ and θ evaluated on a test image.

Figure 9. Schematic of square wave used in Λ evaluation example.

Figure 10. Pdf of θ measured using crossed-plane tomography in a fully turbulent V-flame.

Figure 11. Pdf of ϕ measured using crossed plane tomography in a fully turbulent V-flame. The smooth curve fit is of the form $A\ |\mathbf{N}\bullet\mathbf{n}_y|\ \exp(-\phi^2/\zeta^2)\ \sin\phi$, based on a Gaussian surface weighted joint PDF of ϕ and θ.

Figure 12. Plot of crossing weighted mean inverse cosine term, $\langle 1/|\sigma_y| \rangle_c$, versus Gaussian fit parameter, ζ.

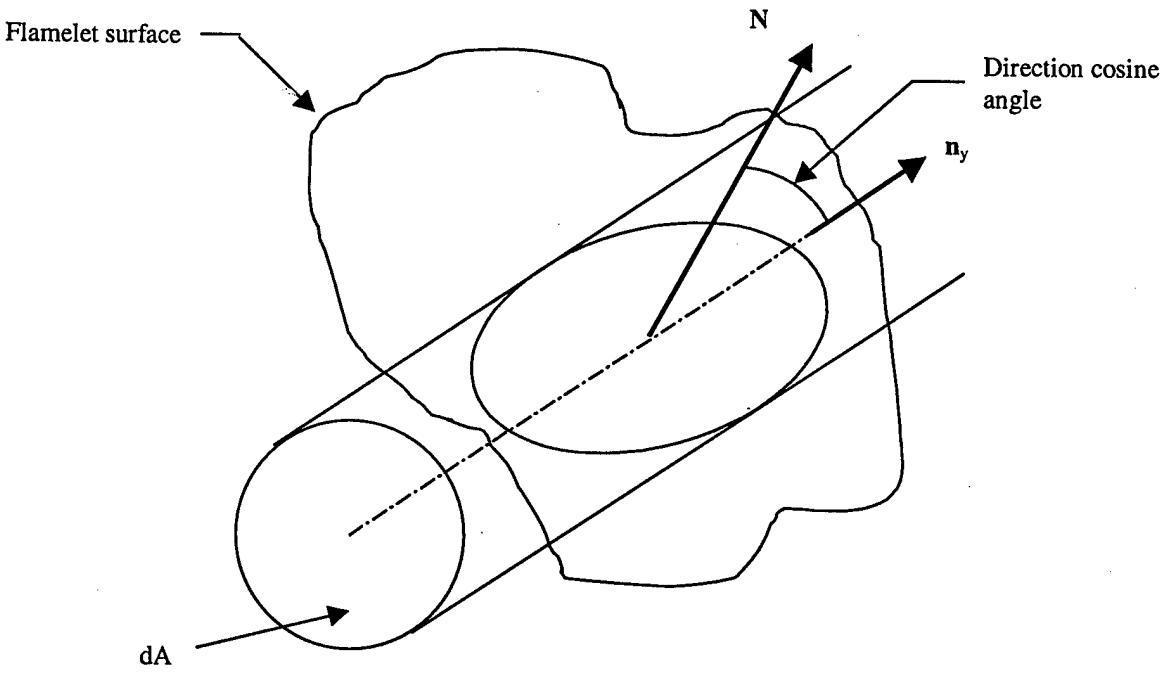

Figure 1

D. A. Knaus, F. C. Gouldin, D. C. Bingham

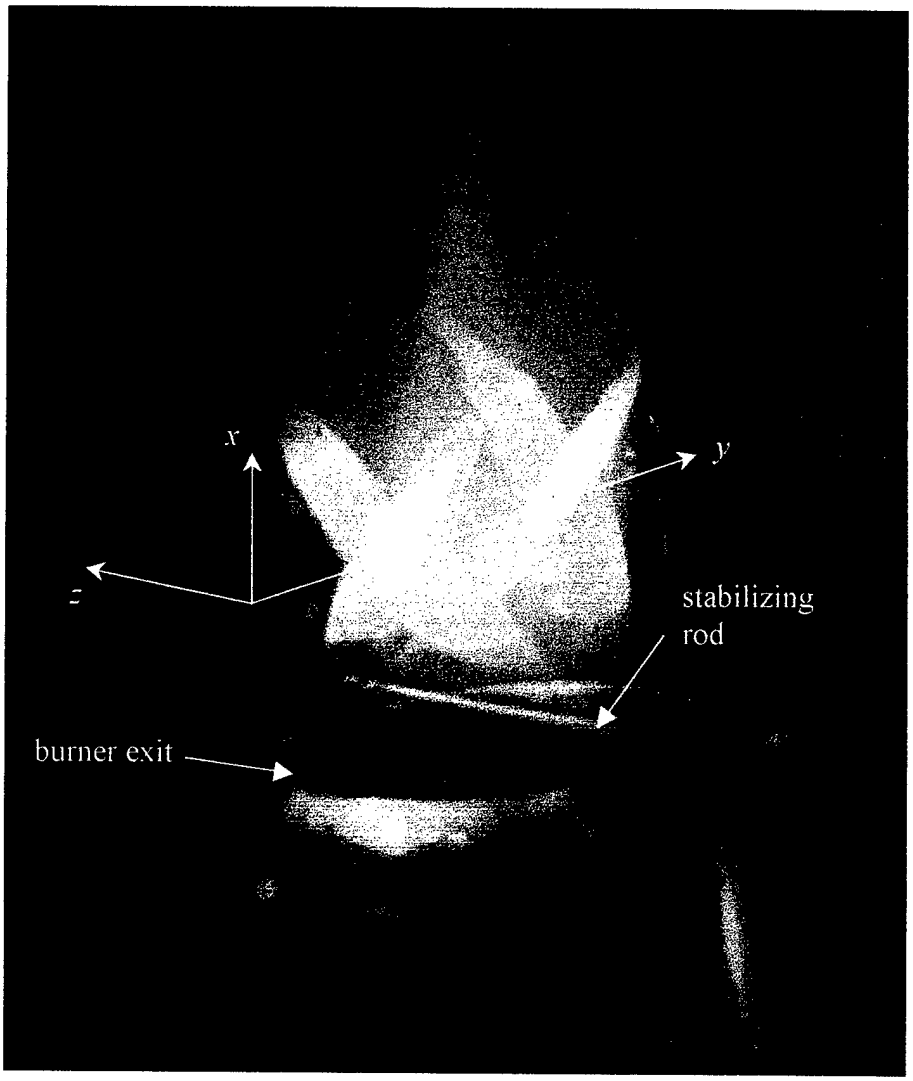

Figure 2

D. A. Knaus, F. C. Gouldin, D. C. Bingham

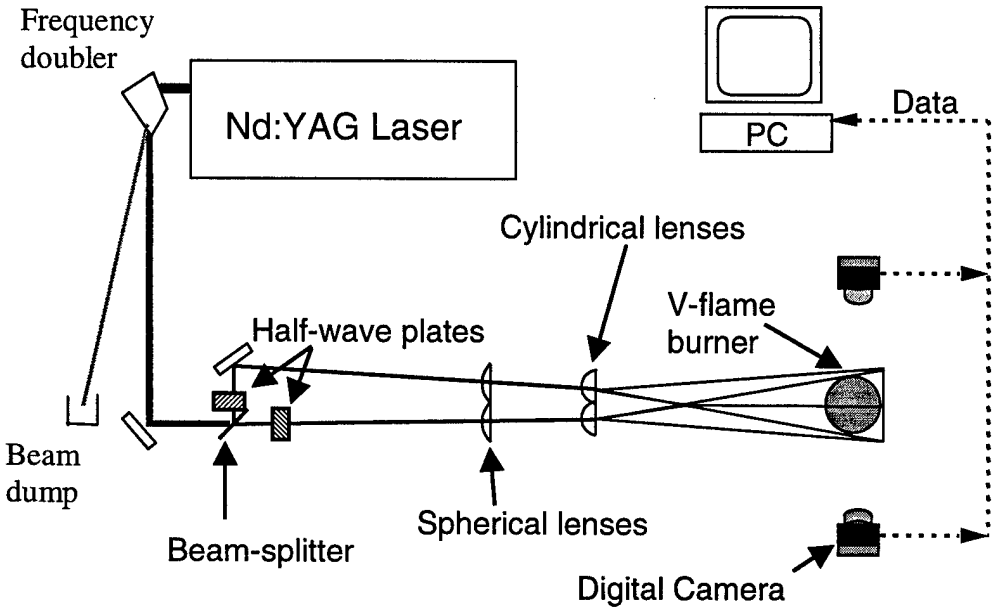

Figure 3

D. A. Knaus, F. C. Gouldin, D. C. Bingham

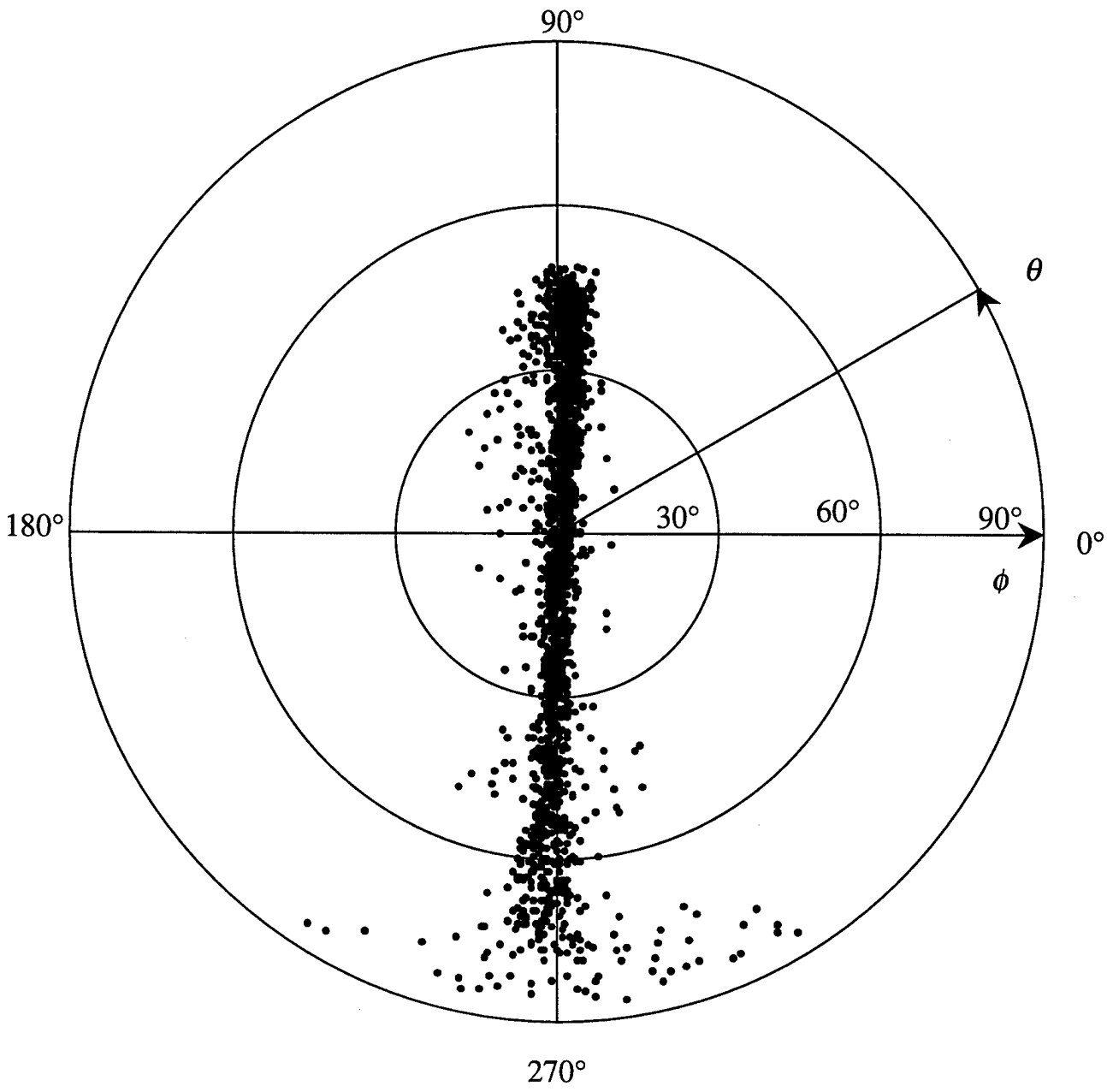

Figure 4

D. A. Knaus, F. C. Gouldin, D. C. Bingham

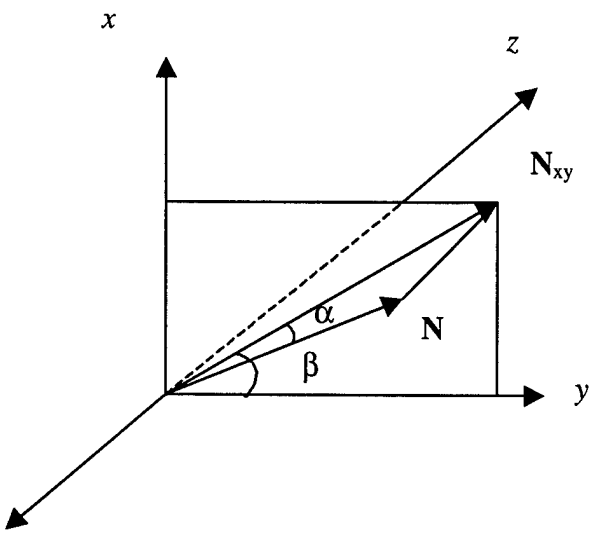

Figure 5

D. A. Knaus, F. C. Gouldin, D. C. Bingham

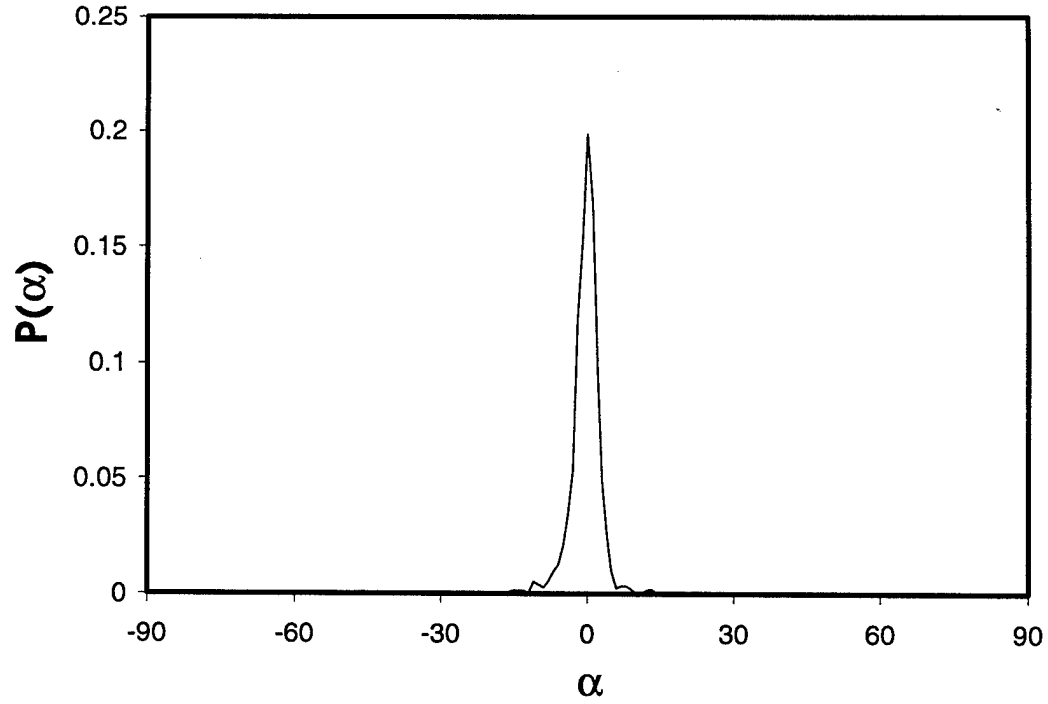

Figure 6

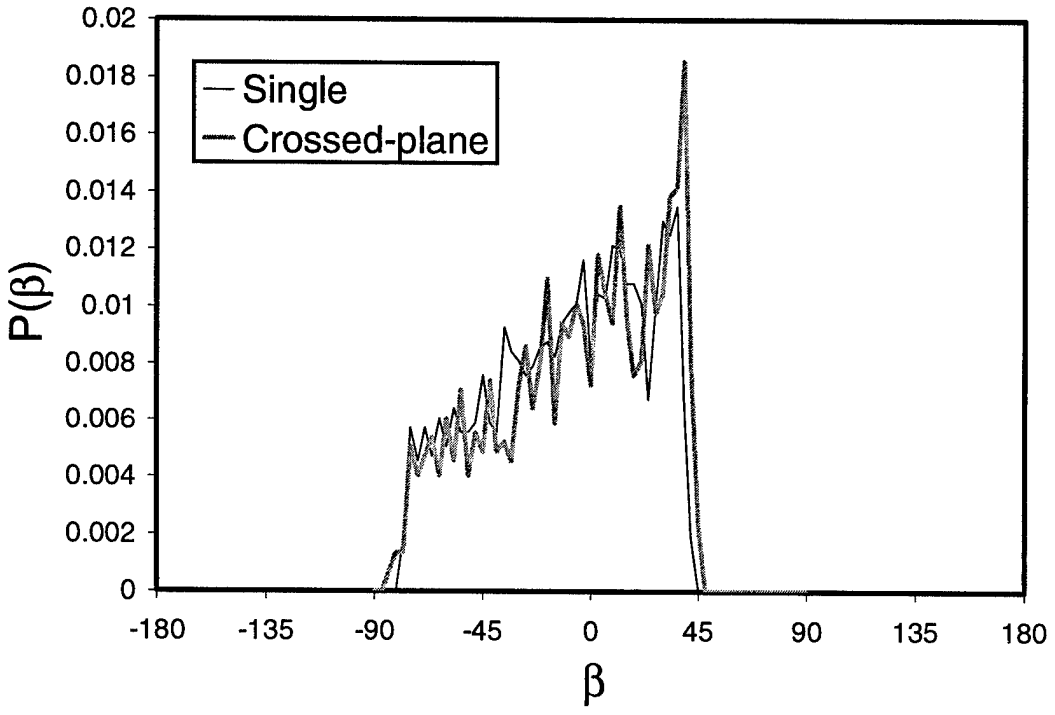

Figure 7

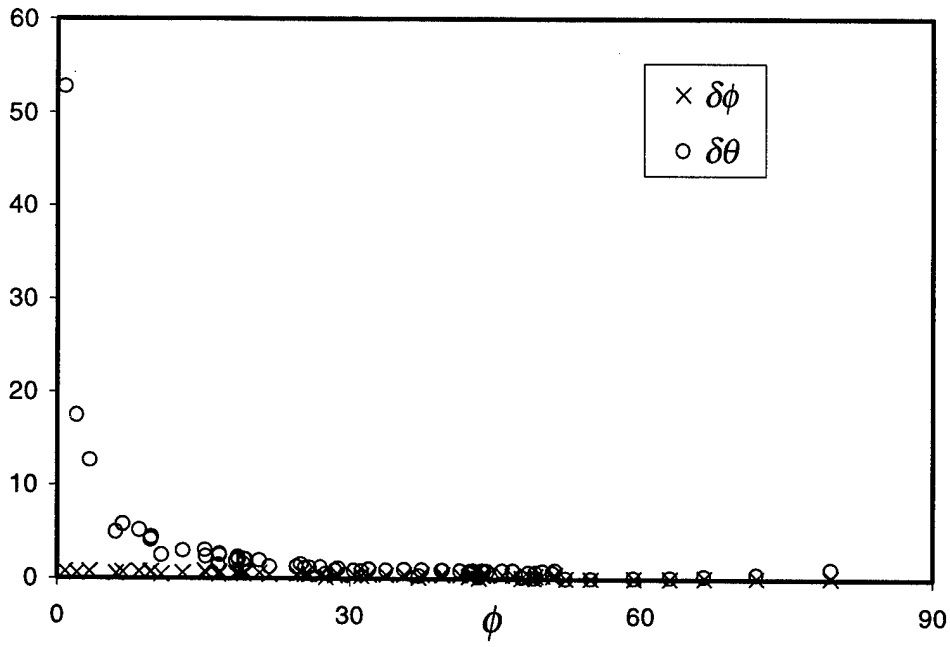

Figure 8

D. A. Knaus, F. C. Gouldin, D. C. Bingham

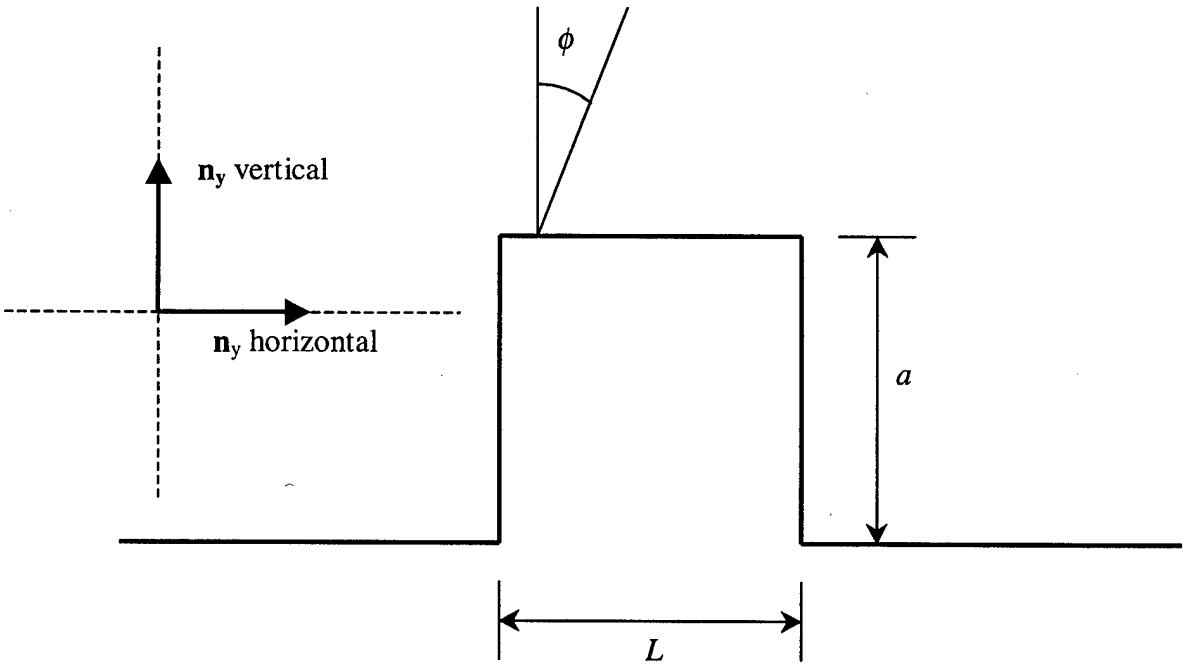

Figure 9

D. A. Knaus, F. C. Gouldin, D. C. Bingham

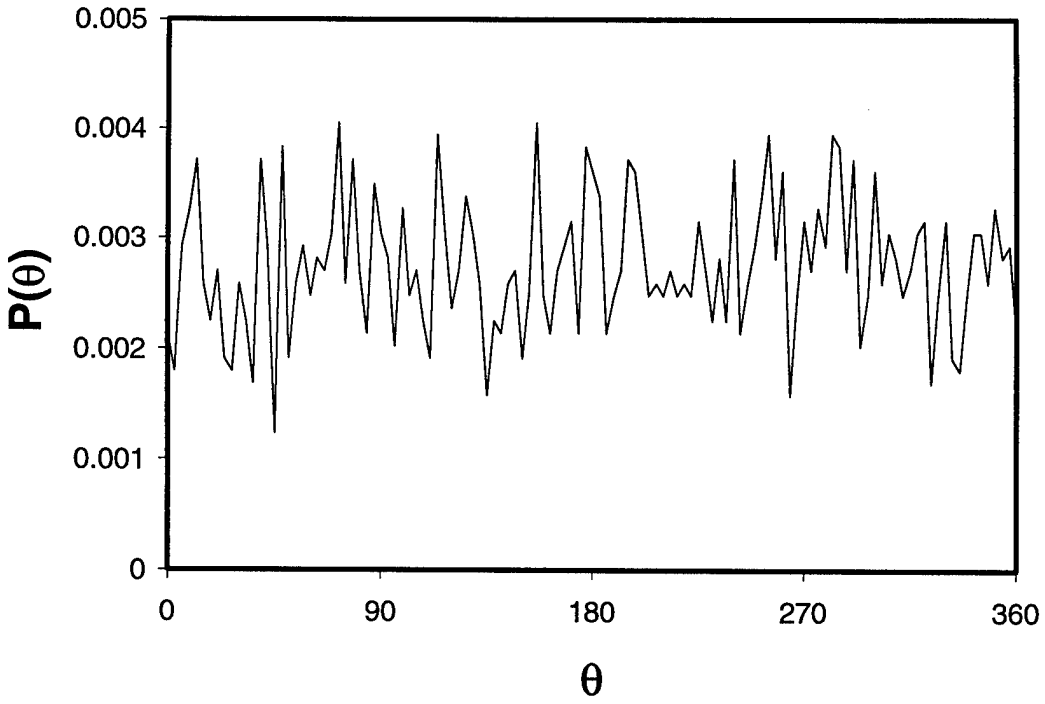

Figure 10

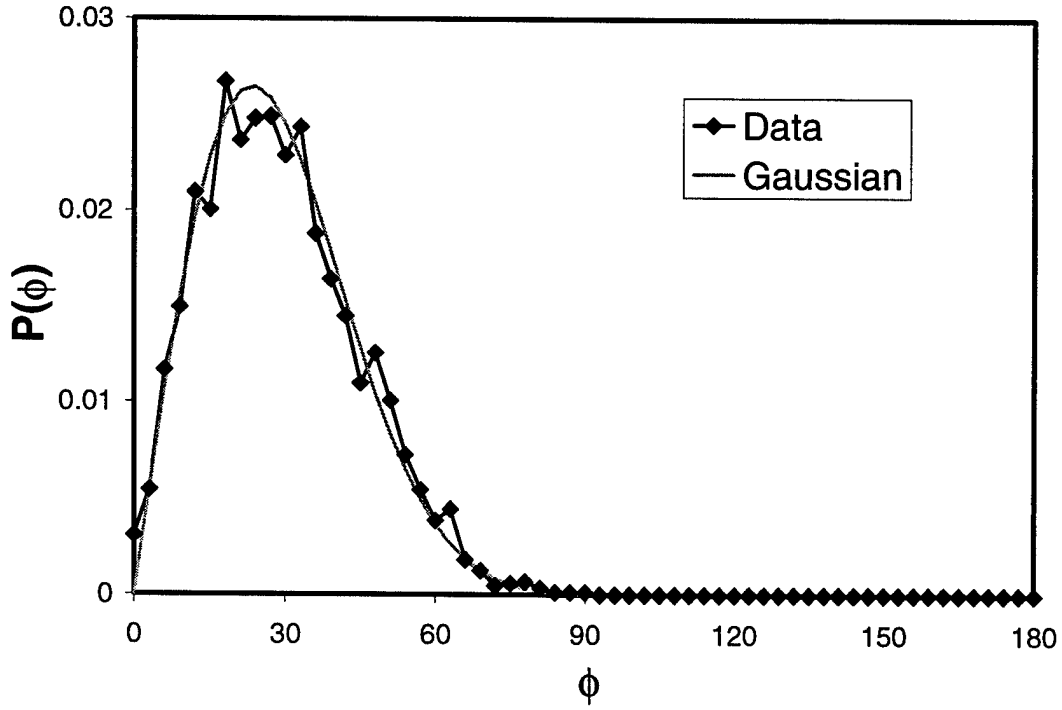

Figure 11

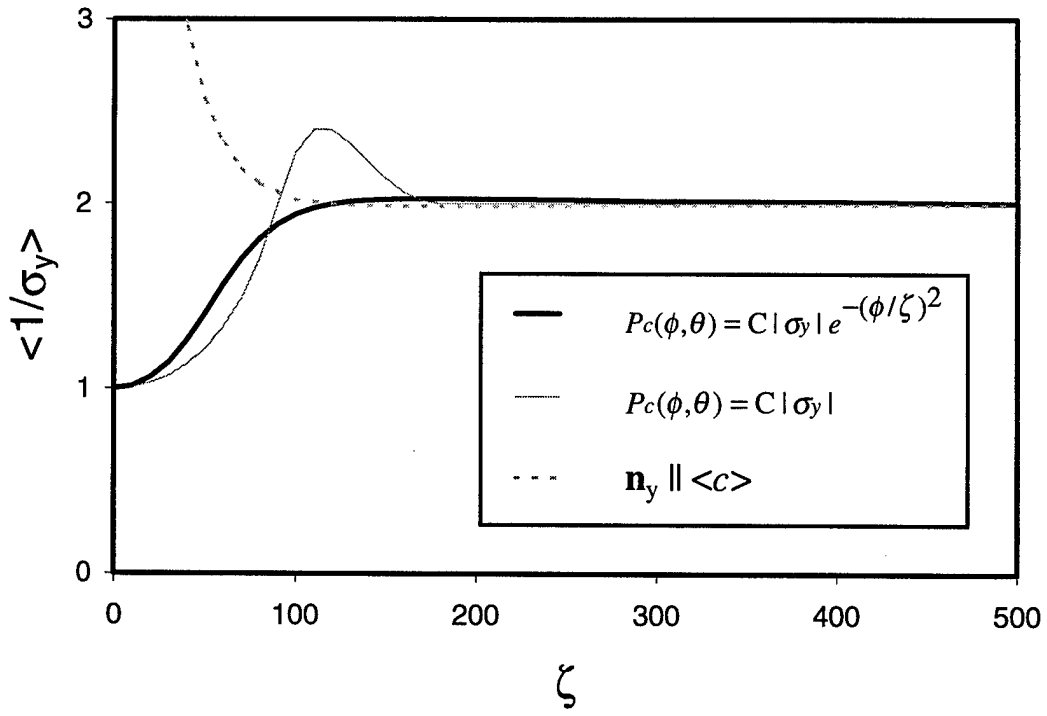

Figure 12

D. A. Knaus, F. C. Gouldin, D. C. Bingham